Heliyon

Received:
7 November 2017
Revised:
10 January 2018
Accepted:
18 June 2018

Cite as: Yassir Elkhidir, Renfa Lai, Zhiqiang Feng. The impact of photofunctionalized gold nanoparticles on osseointegration. Heliyon 4 (2018) e00662. doi: 10.1016/j.heliyon.2018.e00662

The impact of photofunctionalized gold nanoparticles on osseointegration

Yassir Elkhidir, Renfa Lai, Zhiqiang Feng*

Implant Department – Suihua, The First Affiliated Stomatological Hospital of Jinan University, PR China

* Corresponding author.
E-mail address: 2377615699@qq.com (Z. Feng).

Abstract

Objectives: The aims of this study were to create a new surface topography using simulated body fluids (SBF) and Gold Nanoparticles (GNPs) and then to assess the influence of UV Photofunctionalization (PhF) on the osteogenic capacity of these surfaces.

Materials and methods: Titanium plates were divided into six groups All were acid etched with 67% Sulfuric acid, 4 were immersed in SBF and 2 of these were treated with 10 nm GNPs. Half of the TiO_2 plates were photofunctionalized to be compared with the non-PhF ones. Rat's bone marrow stem cells were seeded into the plates and then CCK8 assay, cell viability assay, immunofluorescence, and Scanning electron microscopy (SEM) were done after 24 hours. Gene expression analysis was done using real time quantitative PCR (qPCR) one week later to check for the mRNA expression of Collagen-1, Osteopontin and Osteocalcin. Alkaline phosphatase (ALP) activity was assessed after 2 weeks of cell seeding.

Results: Our new topography has shown remarkable osteogenic potential. The new surface was the most biocompatible, and the 10 nm GNPs did not show any cytotoxicity. There was a significant increase in bioactivity, enhanced gene expressions and ALP activity.

https://doi.org/10.1016/j.heliyon.2018.e00662
2405-8440/© 2018 Published by Elsevier Ltd. This is an open access article under the CC BY-NC-ND license (http://creativecommons.org/licenses/by-nc-nd/4.0/).

Conclusions: GNPs enhances osteogenic differentiation of stem cells and Photofunctionalizing GNPs highly increases this. We have further created a novel highly efficient topography which highly enhances the speed and extent of osseointegration. This may have great potential for improving treatment outcomes for implant, maxillofacial as well as orthopedic patients.

Keywords: Nanotechnology, Biomedical engineering, Dentistry

1. Introduction

Titanium has become the material of choice in many treatment modalities in the dental field [1]. For dental implants, osseointegration (OI) of bone to the implant surface is considered the major criteria of implant's treatment success [2, 3, 4, 5]. Titanium has a high osseointegrative capacity compared to other biomaterials. It can achieve high levels of bone anchorage due to their biocompatibility and excellent mechanical properties, and extensive research has been done to enhance these surface properties. In this study, we combine some of the most recent trends of titanium surface modifications to assess their effect on the OI process.

1.1. Photofunctionalization

Although titanium is the most biocompatible and the most clinically used alloy for orthopedic and dental implants, it was found to be subjected to "biological ageing" in which they encounter time-related degradation of their bioactivity leading to a decrease in their osteoconductivity over time [6, 7, 8, 9, 10, 11, 12, 13, 14, 15, 16, 17, 18, 19, 20, 21, 22, 23, 24]. One of the approaches that have been done to overcome this issue was Photofunctionalization (PhF), a concept described by Takahiro Ogawa [11] in which he used ultraviolet light to alter the physiochemical properties of titanium surfaces and increase the bone-implant contact (BIC) to almost 100%, a phenomenon termed "Superosseointegration". Ultraviolet application to titanium surfaces was shown to effectively reverse the ageing process of titanium caused by the deposition of hydrocarbon on its surface. It also restored the surface charge back to positive and remarkably increased the hydrophilicity of the surface.

On the molecular level, protein absorption, and osteoblastic function becomes highly enhanced leading to an almost ideal surface contact, and therefore better primary stability and substantial therapeutic significance. Photofunctionalization have shown to decreases morbidity and improves treatment outcome by highly increasing the Bone-implant contact leading to a 3-fold increase in the strength of primary stability. It therefore allows for a quicker loading protocol and a decreased overall treatment time. It also permits the use of shorter and smaller implants in complex cases without compromising the success rate [17, 18, 19, 20, 21, 22, 23, 24, 25, 26, 27, 28, 29, 30,

https://doi.org/10.1016/j.heliyon.2018.e00662
2405-8440/© 2018 Published by Elsevier Ltd. This is an open access article under the CC BY-NC-ND license (http://creativecommons.org/licenses/by-nc-nd/4.0/).

31, 32, 33, 34, 35, 36, 37, 38, 39, 40, 41, 42, 43, 44, 45, 46, 47, 48, 49, 50, 51, 52, 53, 54, 55, 56, 57, 58, 59, 60, 61, 62, 63, 64, 65, 66, 67, 68]. Photofunctionalization resulted in similar effects when applied on other alloys as well as non-alloy materials such as zirconium, opening possibilities to further research applications in the field of dental materials. Moreover, this new technology has been applied with different other surface modification techniques such as nanotechnology and stem cell tissue engineering and has shown promising results [32, 69, 70, 71, 72, 73, 74, 75, 76, 77, 78, 79, 80, 81, 82, 83, 84, 85, 86, 87, 88, 89, 90, 91, 92, 93, 94, 95, 96, 97].

1.2. Gold nanoparticles (GNPs)

The unique physical and chemical properties and the high biocompatibility of Gold nanoparticles (GNPs) have made them highly attractive for the use in different medical fields such as targeted gene and drug delivery, diagnostics as well as tissue engineering research [98, 99, 100, 101, 102, 103, 104].

Cellular uptake of GNPs causes them to bind to cytoplasmic proteins and act as osteogenic agents to enhance bone tissue regeneration [105]. Following cellular endocytosis [106, 107], GNPs act as a mechanical stimuli and lead to activation of the p38 mitogen-activated protein kinase signaling pathway (MAPK) which up-regulates the transcription factor (Runx-2) in the nucleus. Runx-2 is the main gene responsible for directing and enhancing osteogenic differentiation of mesenchymal stem cells into osteoprogenitor cells. It induces the expression of other osteoblastic specific genes such as Osteopontin (OPN), Osteocalcin (OCN) and Collagen type I, alpha 1(Col-1) [108, 109, 110, 111] (Fig. 1).

Previous studies have shown that beside these osteogenic capabilities, GNPs also inhibit osteoclast formation [112] as well as adipogenic differentiation [113]. GNPs can therefore be very useful if it is applied on titanium surfaces as a method of surface modification as it can stimulate bone formation and hence, faster implant osseointegration and better primary stability [75]. One recent study found that 28 nm sized GNPs enhances osteogenic differentiation of Adipose Derived Stem Cells and increases the expression of specific markers related to osseous growth. These concluded that these findings suggested that Titanium-GNP (Ti-GNP) have an increased osteoconductive capabilities [114]. Nevertheless, Others have found that the smaller the size of GNPs, the more significant impact on osteogenic differentiation [115].

In this study, 10 nm diameter spherical GNPs were used in order to assess whether this size will promote more osteogenic differentiation than those previously mentioned in the literature.

https://doi.org/10.1016/j.heliyon.2018.e00662
2405-8440/© 2018 Published by Elsevier Ltd. This is an open access article under the CC BY-NC-ND license (http://creativecommons.org/licenses/by-nc-nd/4.0/).

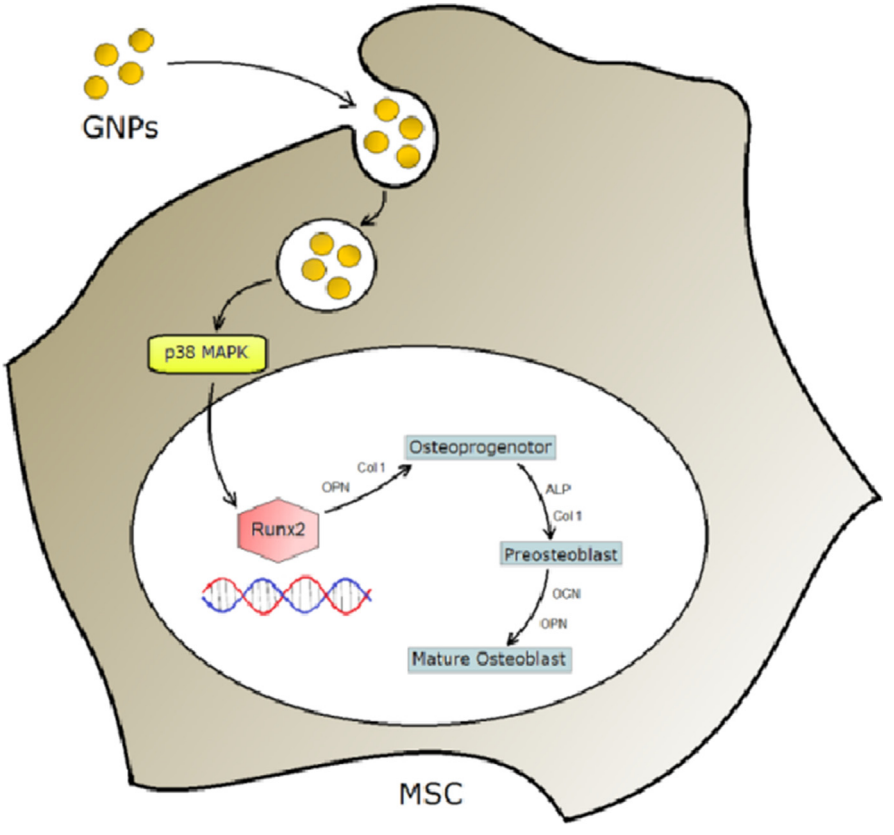

Fig. 1. Endocytosis of GNPs causes them to activate the p38 MAPK pathway which stimulates of the Runx-2 gene leading to osteogenic differentiation.

1.3. Simulated body fluid (SBF)

In order to bond to living bone, it is essential for any biomaterial to form a biomimetic bone-like apatite on the material surface. Simulated body fluid (SBF) is a solution which has an ion concentration close to that found in human blood plasma [116, 117]. The precipitation of calcium and phosphate ions found in SBF causes spontaneous growth of apatite with a similar molecular structure to bone on the surface of biomaterials. Different materials have been immersed in SBF, and it was shown that their in vitro bone bioactivity could be predicted by the extent of resulting apatite formation [118]. Several studies have reported that SBF application on titanium leads to biomimetic deposition of apatite crystals on their surfaces [119, 120, 121]; this formed hydroxyapatite layer highly increases the osteoconductivity of titanium surface and hence, improves the osseointegration process [122, 123]. In our study, we have used SBF alone and with gold nanoparticles and with or without UV light application to assess the extent of tissue growth on the titanium plates.

https://doi.org/10.1016/j.heliyon.2018.e00662
2405-8440/© 2018 Published by Elsevier Ltd. This is an open access article under the CC BY-NC-ND license (http://creativecommons.org/licenses/by-nc-nd/4.0/).

1.4. Mesenchymal stem cells (MSCs)

Stem cells are promising tools in tissue engineering; they are characterised by their ability of self-renewal and their potential to differentiate into various cell lineages from the three germ layers. Mesenchymal stem cells (MSCs) are multipotent cells and have the potential to differentiate into mesodermal cells to form bone, cartilage, skeletal muscles or adipose tissue [124, 125] This process of differentiation is a basic step in promoting regeneration [126]. The abundance of MSCs at the site of bone injury and their ability to suppress the immune response and stimulate bone regeneration [127] makes these cells very influential in the process of osseointegration.

The bone marrow contains a considerable population of MSCs capable of differentiating into bone. The differentiation of these cells into osteogenic progenitor cells can be influenced by many factors [128, 129]. In this in vivo study, we have used rat's bone marrow stem cells (rBMSCs) to evaluate the growth of MSCs on different titanium surface treatment modalities. Cellular differentiation was evaluated by the expression of col-1, OPN and OCN as well as the expression of the Alkaline phosphatase (ALP) activity of the cells.

2. Materials and methods

2.1. Experiment outline

The objective of this study was to assess the cell growth of mesenchymal stem cells (MSCs) obtained from rat's bone marrow stem cells on the surface of titanium (TiO_2) in different conditions. SBF, GNPs and UV PhF were applied to the TiO_2 plates. The main outline of the experiment consisted of six groups of titanium plates, each group has a different modification modality. The groups were named 1A, 2A, 3A, 1B, 2B and 3B. Their surface characteristics were prepared as the following (Fig. 2):

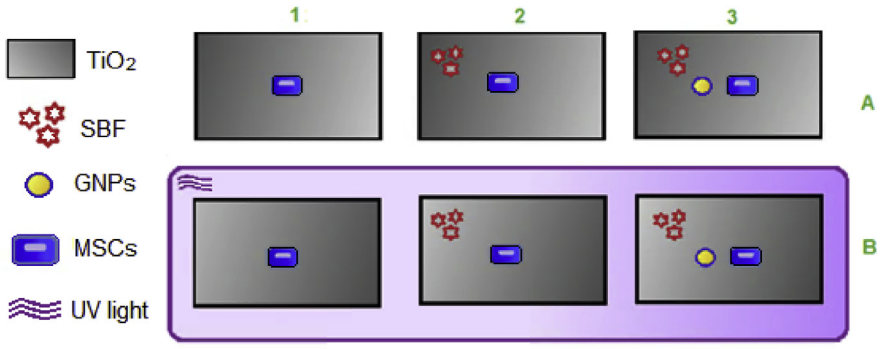

Fig. 2. TiO_2 discs were grouped as follows: 1. MSCs, 2. MSCs and SBF, 3. MSC, SBF and GNPs, A. Non-photofunctionalized group, B. Photofunctionalized group.

https://doi.org/10.1016/j.heliyon.2018.e00662
2405-8440/© 2018 Published by Elsevier Ltd. This is an open access article under the CC BY-NC-ND license (http://creativecommons.org/licenses/by-nc-nd/4.0/).

Group A:

1- (TiO_2 + MSCs),

2- (TiO_2 + MSCs + SBF),

3- (TiO_2 + MSCs + SBF + GNPs)

Group B:

1- (TiO_2 + MSCs + PhF),

2- (TiO_2 + MSCs + SBF + Ph)F,

3- (TiO_2 + MSCs + SBF + GNPs + PhF)

2.2. Processing methods

Commercially pure (99.7%) Titanium grade 4 disks (20*20 mm, 1.5 mm thickness) were obtained (Baoji Rare Titanium Nickel co, Guangzhou, P.R. China). The sequence of processing was acid etching for 30 minutes, SBF for 24 hours, PhF for 48 hours, GNPs for 24 hours, followed by MSCs application on the TiO_2 plates to evaluate their osteogenic differentiation and growth.

2.2.1. Acid etching

All titanium plates were sterilized using a regular autoclave, and then acid-etched with 67% Sulfuric acid (H_2SO_4) at 120 °C for 30 minutes. All plates were then disinfected, washed twice with distilled water and then put into the 6 well cell culture plate.

2.2.2. Photofunctionalization

Group B titanium plates were photofunctionalized by closely exposing them to UV light for 48 hours in a dark box using a 15 W bactericidal lamp; (Toshiba, Tokyo, Japan) with a combined peak intensity of 0.05 mW/cm^2 ($\lambda = 360 \pm 20$ nm) and 2 mW/cm^2 ($\lambda = 250 \pm 20$ nm).

2.2.3. Biomimetic hydroxyapatite deposition and characterization

Simulated Body Fluids from Beijing LEAGENE Biotechnology Co., Ltd (CZ0400), was prepared to mimic the ion concentrations found in human plasma. Titanium plates in groups 2A, 3A, 2B and 3B were soaked in SBF (pH 7.40) at 37 °C for 24 hours prior to the experiment. The disks were then removed and gently washed three times in distilled water for 30 seconds and then air-dried on a clean bench. Surface morphology was then assessed using scanning electron microscopy (SEM).

https://doi.org/10.1016/j.heliyon.2018.e00662
2405-8440/© 2018 Published by Elsevier Ltd. This is an open access article under the CC BY-NC-ND license (http://creativecommons.org/licenses/by-nc-nd/4.0/).

2.2.4. Titanium plates preparation

TiO_2 plates from groups 3A and 3B were immersed in hexane acetone, ethanol and deionized water. They were then ultrasonically cleaned for 15 minutes, dried with nitrogen, soaked in sodium hydroxide solution for 24 hours, washed thoroughly with deionized water and ultrasonically cleaned again. TiO_2 plates were then immersed in toluene solution containing 2% MPTPs at 60 °C for 24 hours, disinfected with ethanol, washed with deionized water and dried with nitrogen. Finally, the plates were immersed in 10 nm GNP solution from Shanghai carboxene biopharmaceutical Technology Co., Ltd (Au01002) at 37 °C for 24 hours, thoroughly cleaned with deionized water and then put into the 6-well plate.

2.2.5. Rat bone marrow stem cells (rBMSCs) isolation and culture

All procedures employed in this study involving animals and their care were conducted in accordance to the National Institutes of Health guidelines (NIH Publication No. 85−23, revised 1996) and were approved by the Wuhan University Animal Care and Use Committee.

2.2.5.1. Isolation

Healthy 6−8 week old Sprague Dawley (SD) rats (4 SPF) were purchased from animal experimental center of Zhongnan Hospital of Wuhan University; L-DMEM medium (Dulbecco's Modified Eagle's medium), fetal bovine serum, trypsin, penicillin and streptomycin from (Procell); 100 mm plastic cell culture dishes from (Corning, USA); Inverted phase contrast microscope from (Olympus, Japan).

SD rats anesthetized with 10% chloral hydrate. 75% ethanol disinfection was done for 10 minutes twice and both lower limbs and lower abdominal area were cut with sterile scissors. Lower limb skin was cut. Legs, thighs, thigh muscle and bone were removed. Femur was exposed and hip joint and knee joint were cut. Then the bilateral femur and tibia were removed under sterile conditions, followed by the bone surface muscle and periosteum. Femur and tibia were separated into a sterile petri dish and sterilized by flushing the bone three times with a sterile solution containing 5% PBS penicillin and streptomycin, and 1% mycillin. Washing was repeated by soaking in large 50 ml centrifuge tube. When the liquid was completely soaked the bones, rongeur metaphysis was applied, using a needle pulling 5 ml culture system (L-DMEM medium +100 U/mL penicillin and streptomycin + 2 mML-glutamine + 7.5% $NaHCO_3$ + 10% FBS). Bone marrow was isolated, percussion with pipettes, made into single cell suspension adding PBS at 1600 rpm for 5 min followed by centrifugal elutriation twice. The density gradient centrifugation

https://doi.org/10.1016/j.heliyon.2018.e00662
2405-8440/© 2018 Published by Elsevier Ltd. This is an open access article under the CC BY-NC-ND license (http://creativecommons.org/licenses/by-nc-nd/4.0/).

isolated the cell suspension in a L-DMEM1:5 dilution. Lymphocytes of rats were placed in a separate volume Liquid. The liquid layered Percoll (density 1.073 g/mL), placed in the centrifuge at 1600 r/min for 15 min. A ring with a middle brown cloudy layer of cells (mononuclear cell layer) were formed. It was washed with PBS twice, centrifuged for 10 min at 1600 r/min, supernatant was discarded, and then 10 mL L-DMEM medium was added into a single cell suspension and then inoculated in 100 mm cell culture dish at 37 °C and 5% CO_2 hatch.

2.2.5.2. Cell culture

Following 48 h of primary culture, the medium was replaced by a fresh medium. Then the cells were covered with the bottom of the culture bottle and they were fused into a single layer. The density of the cells was 70%−80%. Cell passaging was carried out with the ratio of 1:2.

Cells where seeded on all titanium plates. MEM- alpha was added to 10 % FBS and 1% Penicillin-Streptomycin Solution. When the cell density reached 80%, the cells were passaged. The culture medium was then discarded and washed with PBS and 1−2 ml 0.25% trypsin. Separation of cells was observed under the microscope till they became rounded indicating complete digestion. Pancreatin was discarded and the cells were put into a single cell suspension and then passaged according to the ratio of 1:3 at 37 °C and 5% CO_2 in saturated humidity conditions to expand cultivation. Light microscopy was used to assess proliferation.

2.3. Tests

2.3.1. CCK8 test and spectrophotometry

The cell counting kit (CCK-8) was performed to determine the extent of the MSCs viability after 24 hours of cell culture with the different TiO_2 modification modalities. Following one day of incubation the absorbance on bare titanium with no modification (1A) was fixed at 100% as a control and spectrophotometry was done. The optical density (OD) of all groups were compared to 1A.

Cell counting kit (CCK8) was applied to each well by adding of 300 ml of the solution for 4 h, and then another 100 ul was added to each of the 5 holes in every group of titanium plates. The mortality rate was measured in each hole by OD450 standard enzyme. spectrophotometry was then done do check for the optical density.

2.3.2. Dead/live assay

Confocal laser scanning microscopy was used to examine cell viability in hBMSCs seeded onto titanium surfaces. After 24 h of culture, the cells were fixed

https://doi.org/10.1016/j.heliyon.2018.e00662
2405-8440/© 2018 Published by Elsevier Ltd. This is an open access article under the CC BY-NC-ND license (http://creativecommons.org/licenses/by-nc-nd/4.0/).

in 10% formalin and stained using the fluorescent dye calcein-AM (Green) for live cells and Propidium iodide (red) for dead cells. Using fluorescent images, each TiO_2 group were assessed for four different plates and they were then averaged together.

2.3.3. Immunofluorescence

Morphology and morphometry of cells on TiO_2 surfaces of all groups were examined after 24 hours following cell seeding to evaluate the cellular spreading and cytoskeletal arrangement of the cultured cells using confocal laser scanning microscopy. Cells were fixed in 10% formalin and confocal microscopic images of cells stained with 4′,6-diamidino-2-phenylindole (DAPI) to detect the nucleus (keygentec), anti-vinculin to detect vinculin protein within the cytoplasm (Proteintech), and rhodamine phalloidin for actin filaments (beyotime.inc).

2.3.4. Surface characterization

Scanning electron microscope (S2300, Hitachi, Japan) was used after 24 hours of seeding the cells on the plates to examine the surface topographies of the titanium plates as well as the cellular morphology in each group. 1500, 3000 and 5000 magnifications were used for observation.

2.3.5. PCR gene expressions

2.3.5.1. Real time fluorescence quantitative PCR detection mRNA

Extraction of RNA was done using TRIzol™ reagent, the excess PBS was washed off, rinsed twice, then 1 ml of TRIzol™ was added to cells followed by to 1.5 ml RNase in the EP tube for 10 min and 200 ul chloroform and mixed thoroughly several times in room temperature for 5 minutes. It was then centrifuged for 15 minutes at 12000 rpm till the RNA was visible under the third phase. The upper aqueous phase (about 400 ul) was transferred into a new 1.5 ml EP tube. 400 ul isopropyl alcohol was added, mixed well, placed at room temperature for 10 min and then centrifuged at 12000 rpm for 10 minutes. The bottom of the tube was seen white due to RNA precipitation. Excess liquid was discarded and RNase of 75% ethanol 1 ml was added, mixed and centrifuged again for 5 minutes at 10000 rpm. The RNA precipitation was air dried for 5−10 minutes and then dissolved and diluted in 20 ul DEPC solution. Optical density (OD) was calculated. The OD260, OD280 and OD260/OD280 values were determined by UV spectrophotometer, and the purity and concentration of RNA were calculated. According to the ratio of OD260/OD280, the quality of RNA was estimated, and the ratio was between 1.8 and 2.0. The absorbance value was calculated according to the following formula the concentration of the sample RNA: Total RNA

https://doi.org/10.1016/j.heliyon.2018.e00662
2405-8440/© 2018 Published by Elsevier Ltd. This is an open access article under the CC BY-NC-ND license (http://creativecommons.org/licenses/by-nc-nd/4.0/).

concentration (ug/ul) = OD260 * 40 * 200 * 10-3. The total RNA was placed in the refrigerator at −80 °C for storage.

2.3.5.2. Reverse transcription into cDNA

Reagents: 2.576 ul RNA, 2 ul of Oligo (dT) 15 (10 uM), 2 ul of dNTP (2.5 mM) and up to 14.5 ul of ddH_2O (RNase free). Reaction conditions were 70 °C for 5 min, following a brief centrifugation on the ice. All were put in the PCR tube (14.5 ul) and added with 4 ul of 5×RT buffer, 0.5 ul of RNase Inhibitor. 1 ul of M-MLV reverse transcriptase and Up to 20 ul of ddH_2O (RNase free). *Reaction conditions* for this were 42 °C for 60 minutes and 95 °C for 5 minutes.

2.3.5.3. Semi quantitative RT-PCR detection

Reagents: 0.5 ul Reference F (10 uM), 0.5 ul Reference R (10 uM), 2 ul dNTP (2.5 mM), 0.25 ul Ex Taq, 2.5 ul 10×Ex Taq E buffer, 1 ul cDNA and Up to 25 ul ddH_2O.

Reaction condition: 4 minutes at 94 °C; 30 seconds at 94 °C, 30 seconds at 56 °C, 25 seconds at 72 °C, and then 30 cycles for 4 minutes at 72 °C.

2.3.5.4. Real time fluorescent quantitative PCR detection

Reagents: 4 ul of cDNA was diluted 10 times, then added to 0.4 ul Forward Primer (100 uM), 0.4 ul Reverse Primer (100 uM), 10 ul SYBR Green/Fluorescein qPCR Master Mix (2×), and 2 ul H_2O_5. *Reaction condition:* 0 °C for 2 minutes, 95 °C for 10 minutes; 95 °C for 30 seconds, 60 °C for 30 seconds, 40 cycles. 50 °C minutes, 95 C 10 minute as; 95 °C for seconds 30, 60 °C for 30 seconds. For the dissolution curves, the final data were analyzed by $2^{-\triangle\triangle Ct}$.

2.3.5.5. Primer sequence table

The primer sequence for different markers is shown in (Table 1).

Table 1. Primer sequence for Col-1, OCN and OPN.

Name	Primer	Sequence	Size
b-actin	Forward Reverse	5′- CACGATGGAGGGGCCGGACTCATC -3′ 5′- TAAAGACCTCTATGCCAACACAGT -3	240 bp
Rat Col I	Forward Reverse	5′-TGACTGGAAGAGCGGAGAGT -3′ 5′-GAATCCATCGGTCATGCTCT-3	202 bp
Rat OCN	Forward Reverse	5′- TCATGTCCAAGCAGGAGGGCAGTAA-3′ 5′- TTGTAGGCGTCCTGGAAGCCAATGT -3	175 bp
Rat OPN	Forward Reverse	5′-CCCGATGCCACAGATGAG -3′ 5′-TCCCGTTGCTGTCCTGAT -3	121 bp

https://doi.org/10.1016/j.heliyon.2018.e00662
2405-8440/© 2018 Published by Elsevier Ltd. This is an open access article under the CC BY-NC-ND license (http://creativecommons.org/licenses/by-nc-nd/4.0/).

2.3.6. Alkaline phosphatase activity assay

Alkaline phosphatase (ALP) activity was assessed after two weeks of cell seeding into the titanium plates and was evaluated as the amount of p-Nitrophenyl Phosphate (PNPP) released by the enzymatic reaction at specific areas in a photo of the titanium plates. It was measured using the use of IPP6.0 software.

2.4. Statistical analysis

Graphpad prism 5.0 was used to perform the statistical analysis in this study. The One-way analysis of variance (One-way ANOVA) was used to compare between the results of different TiO_2 groups either by using Bonferroni's Multiple Comparison Test for multiple comparisons or by Dunnett's Multiple Comparison Test to compare between TiO_2 results with the control group 1A. Unpaired one-tailed t-tests were performed separately for comparison between the results of two separate groups.

3. Results

3.1. Cell count and optical density (OD)

3.1.1. Spectrophotometry

The optical density (OD) was measured and cell count was performed and then calculated in percentages compared to 1A (Table 2) and plotted in (Fig. 3).

3.1.1.1. Statistical analysis

One-way ANOVA was used to perform statistical analysis. Bonferroni's Multiple Comparison Test between each two groups revealed that there is a statistical significant increase in cellular count when adding SBF, GNPs and UV light treatment to the titanium plates. The only two non-significant differences were between 1A vs 2A and 3A vs 2B (Table 3).

Table 2. Cell count was performed in 5 separate TiO_2 plates of each group. 3B (GNP + SBF + PhF) showed maximum cellular proliferation compared to the other TiO_2 surfaces.

TiO_2 group	1	2	3	4	5	Average
1A	100.00%	101.29%	101.29%	101.93%	99.36%	**100%**
2A	110.30%	101.29%	112.87%	100.64%	107.72%	**106%**
3A	125.10%	133.46%	127.67%	125.10%	120.59%	**126%**
1B	116.73%	114.16%	117.37%	116.09%	116.09%	**116%**
2B	134.11%	131.53%	132.82%	129.60%	132.82%	**132%**
3B	146.98%	152.12%	143.11%	150.84%	154.70%	**149%**

https://doi.org/10.1016/j.heliyon.2018.e00662
2405-8440/© 2018 Published by Elsevier Ltd. This is an open access article under the CC BY-NC-ND license (http://creativecommons.org/licenses/by-nc-nd/4.0/).

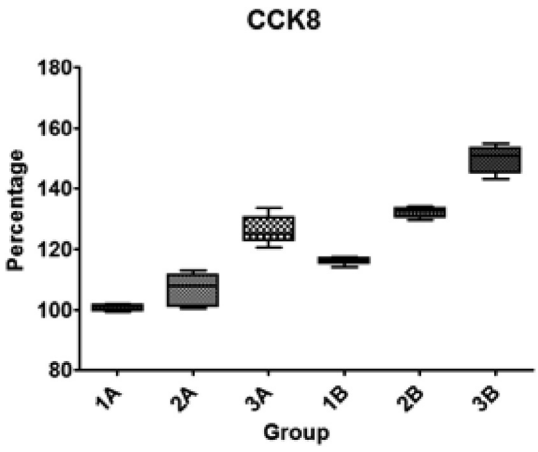

Fig. 3. Cell growth ratio and standard deviation (SD) on different TiO_2 modified surfaces compared to the control group (1A) which was set at 100%. UV treated groups showed higher cellular density in general, and Group 3B showed the highest density.

Table 3. Bonferroni's Multiple Comparison Test between different optical densities. Significance level is indicated by*.

Bonferroni's Multiple Comparison Test	Mean diff.	t	Significance P < 0.05	Summary	95% CI of diff
1A vs 2A	−5.790	2.369	No	ns	−13.93 to 2.352
1A vs 3A	−25.61	10.48	Yes	***	−33.75 to −17.47
1A vs 1B	−15.31	6.265	Yes	***	−23.46 to −7.172
1A vs 2B	−31.40	12.85	Yes	***	−39.54 to −23.26
1A vs 3B	−48.78	19.95	Yes	***	−56.92 to −40.63
2B vs 3B	**−17.37**	**7.107**	**Yes**	***	**−25.52 to −9.232**

2B vs 3B: T-test revealed that there is a significantly high increase in the OD of 3B compared to 2B with P value < 0.0001.

3.2. Cell viability assay (live/dead assay)

PhF and GNPs increase the cellular viability (Fig. 4), The percentage of viable cells was counted. The ratio of live cells was found to increase in the TiO_2 plates in the following order 1A, 2A, 3A, 1B, 2B, 3B (Table 4). The ratio with the standard deviations of all groups was plotted in (Fig. 5).

3.2.1. Live/dead assay results

3.2.1.1. Statistical analysis

Statistical analysis shows that the live/dead ratio is significantly higher in UV treated groups than the non UV treated ones (Table 5).

https://doi.org/10.1016/j.heliyon.2018.e00662
2405-8440/© 2018 Published by Elsevier Ltd. This is an open access article under the CC BY-NC-ND license (http://creativecommons.org/licenses/by-nc-nd/4.0/).

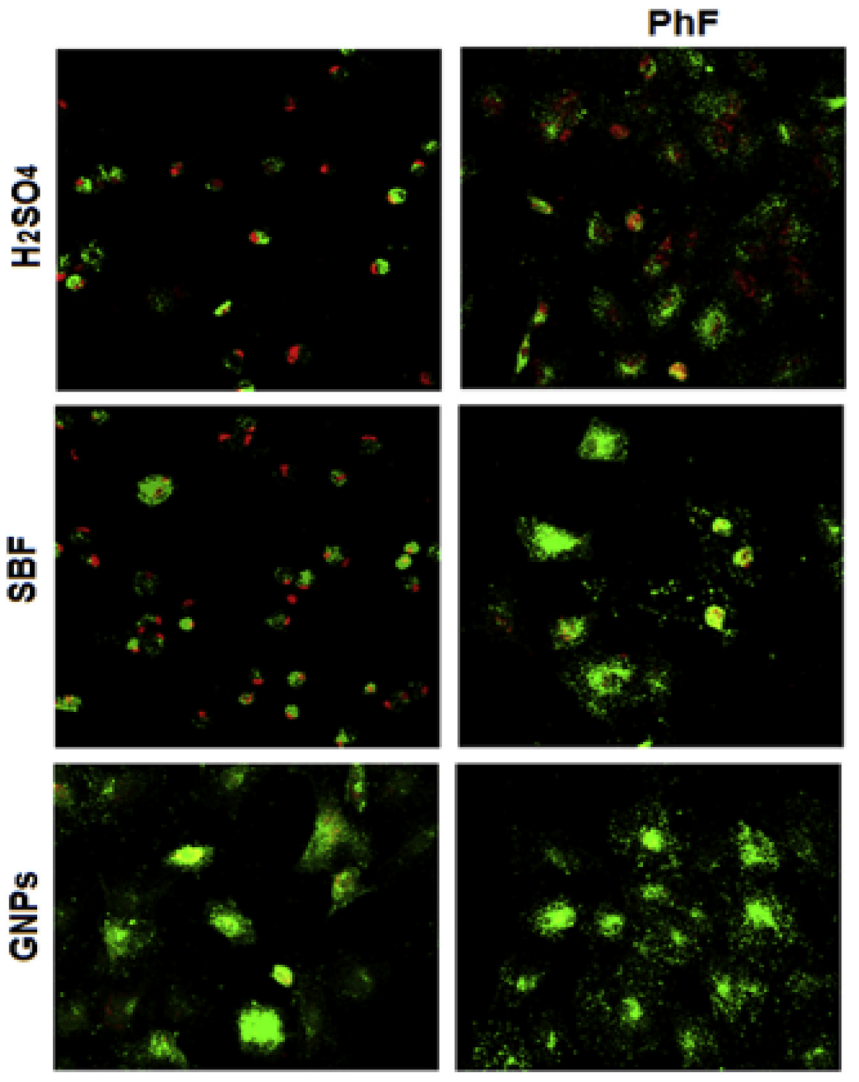

Fig. 4. All PhF TiO_2 surfaces showed higher cellular viability when compared to the non-PhF ones. In both UV treated and non treated groups, the viability in comparison was GNPs > SBF > H_2So_4.

Table 4. Live/dead assay shown by the average percentage of live cells from the total cell count.

	1	2	3	4	Average
1A	48.84	49.06	54.39	49.18	50.37%
2A	53.73	55.10	54.12	57.89	55.21%
3A	60.00	59.26	64.52	60.61	61.10%
1B	70.00	60.71	63.41	64.15	64.57%
2B	78.26	72.22	67.50	60.98	69.74%
3B	82.35	81.82	79.17	73.33	79.17%

https://doi.org/10.1016/j.heliyon.2018.e00662
2405-8440/© 2018 Published by Elsevier Ltd. This is an open access article under the CC BY-NC-ND license (http://creativecommons.org/licenses/by-nc-nd/4.0/).

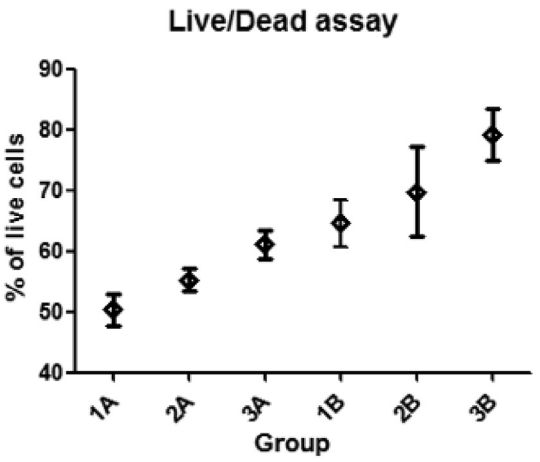

Fig. 5. The ratio of live cells in different TiO_2 groups, with the standard deviation (SD).

Table 5. Dunnett's Multiple Comparison Test for cell viability between different TiO_2 groups. T test was preformed for 2B and 3B. Significance level is indicated by*.

Dunnett's Multiple Comparison Test	Mean diff.	q	Significance P < 0.05 (t-test)	Summary	95% CI of diff
1A vs 2A	−4.897	1.677	No	ns	−12.96 to 3.167
1A vs 3A	−10.79	3.693	Yes	**	−18.85 to −2.721
1A vs 1B	−14.26	4.882	Yes	***	−22.32 to −6.191
1A vs 2B	−19.43	6.653	**0.0156**	***	−27.49 to −11.36
1A vs 3B	−28.86	9.881	**0.0147**	***	−36.92 to −20.79

**B2 vs B3:* Unpaired t test: shows that there is a significant increase in viability in 3B compared to 2B with a P value of 0.0330.

3.3. Morphology and morphometry of cells

The OD of Actin and vinculin are good indicators for cytoskeletal development. The pattern of actin and vinculin expression was as the following:

1B > 1A, 2B > 2A, and 3B > 3A. The expression of actin and vinculin was found to increase in the titanium plates in the following order 1A, 2A, 1B, 3A, 2B, 3B (Fig. 6).

3.3.1. Optical density (OD) calculations

IPP6.0 software was used for the analysis of the optical density of fluorescent photographs, each group had three TiO_2 plates analyzed, optical density analysis per area was calculated for the integral optical density (IOD). The average OD were then calculated (Table 6) and (Fig. 7).

https://doi.org/10.1016/j.heliyon.2018.e00662
2405-8440/© 2018 Published by Elsevier Ltd. This is an open access article under the CC BY-NC-ND license (http://creativecommons.org/licenses/by-nc-nd/4.0/).

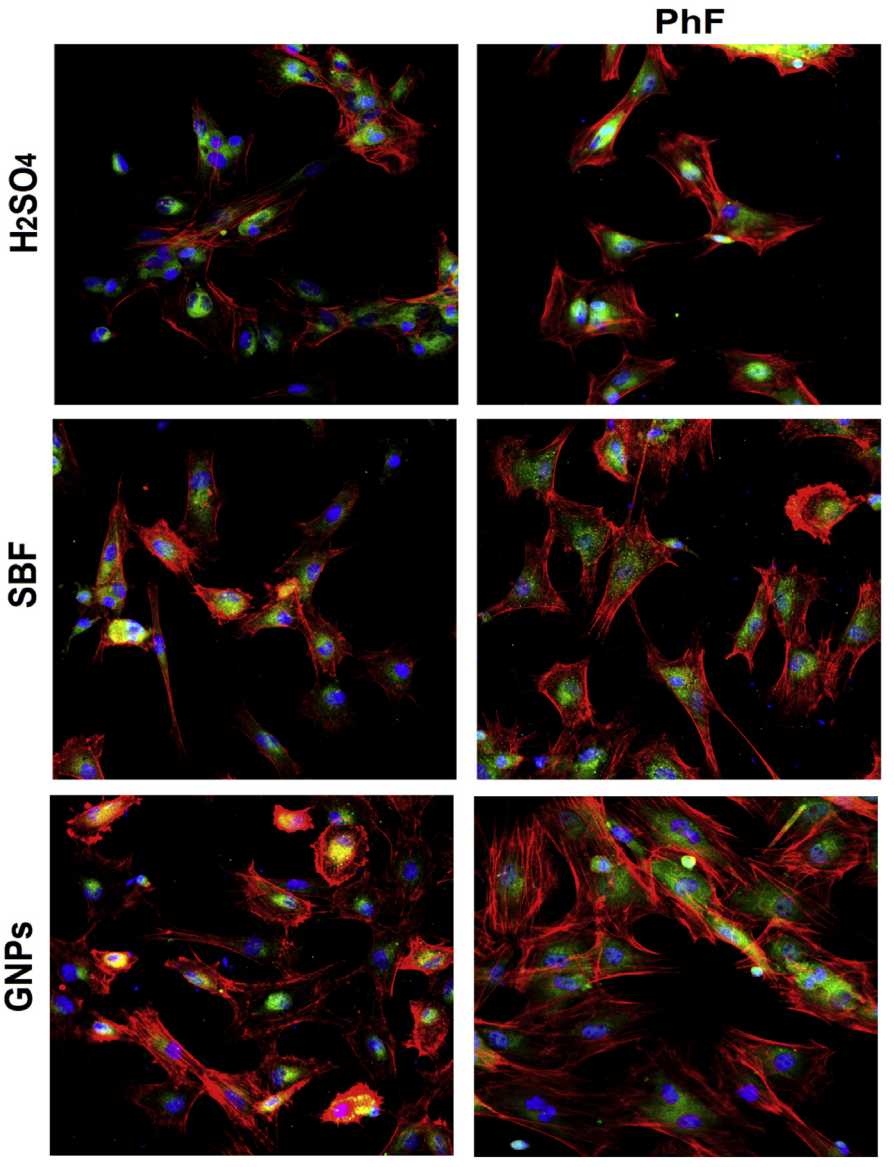

Fig. 6. PhF treated titanium expressed higher stress fibers development, cytoskeletal maturation as well as higher differentiation and cellular density than those with no PhF treatment. The cellular growth and development was GNPs > SBF > H_2SO_4.

Table 6. Average optical density of actin and vinculin for different TiO_2 groups.

Group	Average OD of F-actin	Average OD of vinculin
1A	0.06132	0.05135
1B	0.06958	0.06033
2A	0.06608	0.05608
2B	0.08210	0.07518
3A	0.07508	0.06690
3B	0.08518	0.07911

https://doi.org/10.1016/j.heliyon.2018.e00662
2405-8440/© 2018 Published by Elsevier Ltd. This is an open access article under the CC BY-NC-ND license (http://creativecommons.org/licenses/by-nc-nd/4.0/).

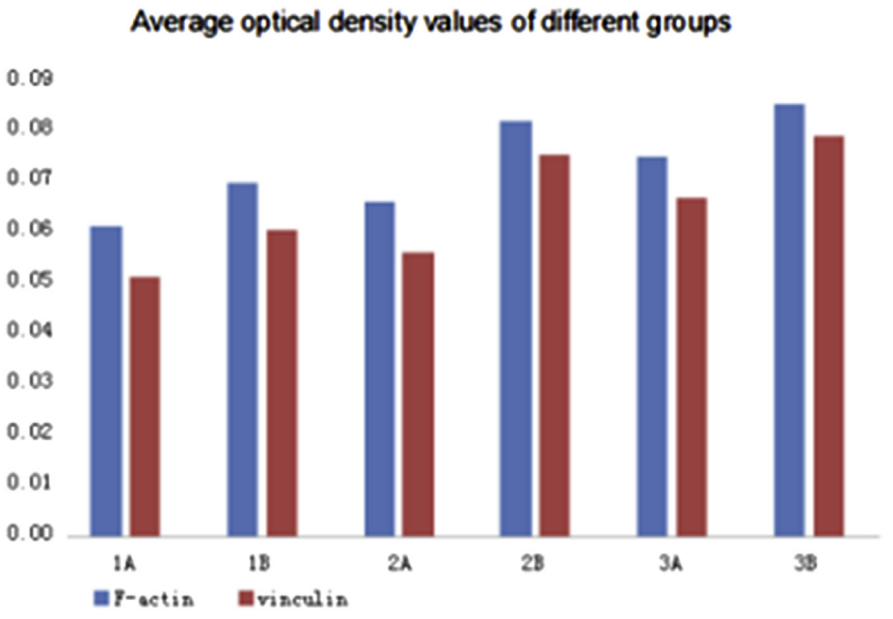

Fig. 7. UV treated groups show enhanced expression of actin and vinculin.

3.4. Surface characterization using scanning electron microscopy (SEM)

SEM was preformed 24 hours following seeding the cells onto the TiO_2 plates to check for surface morphology. The acid-etched titanium plates were of uniform roughness with about 2 um pits as can be seen in 1A and 1B (Fig. 8a). SBF coated plates (2A and 2B) shows the hydroxyapatite layer at higher magnification (Fig. 8b). Both PhF treated (Fig. 9) and GNP treated (Fig. 10) SBF surfaces showed enhanced cellular differentiation. The osteoblasts showed a more defined filopodia and lamellipodia attached to the TiO_2 surface. The PhF groups in general show high increase

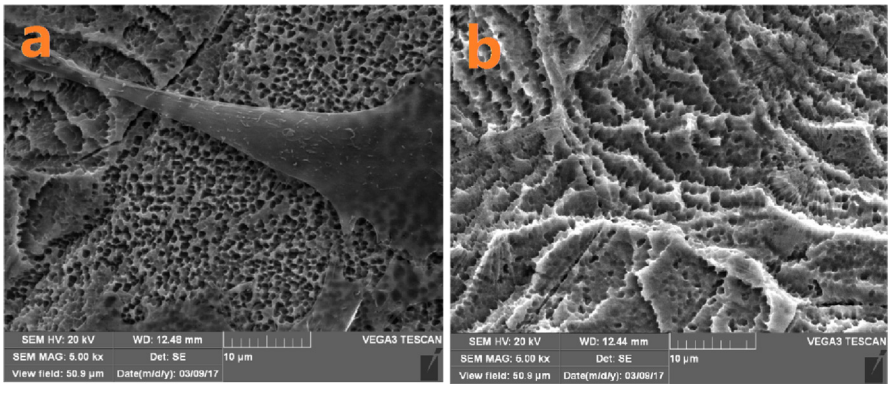

Fig. 8. a) acid etched TiO_2. b) SBF-modified showing the hydroxyapatite layer covering the TiO_2 surface.

https://doi.org/10.1016/j.heliyon.2018.e00662
2405-8440/© 2018 Published by Elsevier Ltd. This is an open access article under the CC BY-NC-ND license (http://creativecommons.org/licenses/by-nc-nd/4.0/).

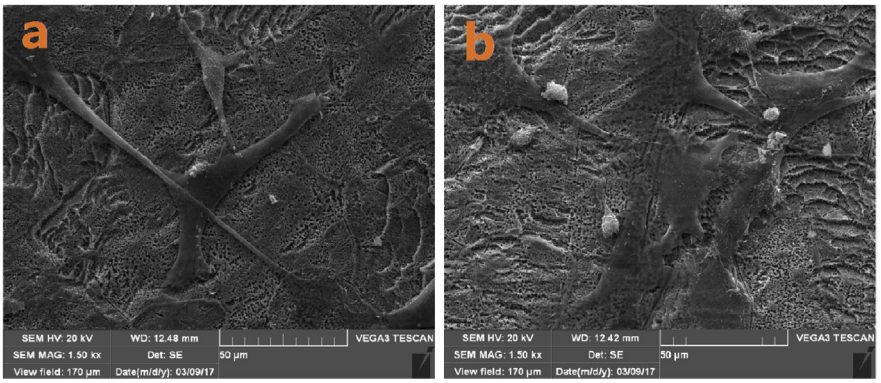

Fig. 9. a) SBF-treated none PhF surface, b) SBF-treated PhF surfaces show higher cellular differentiation.

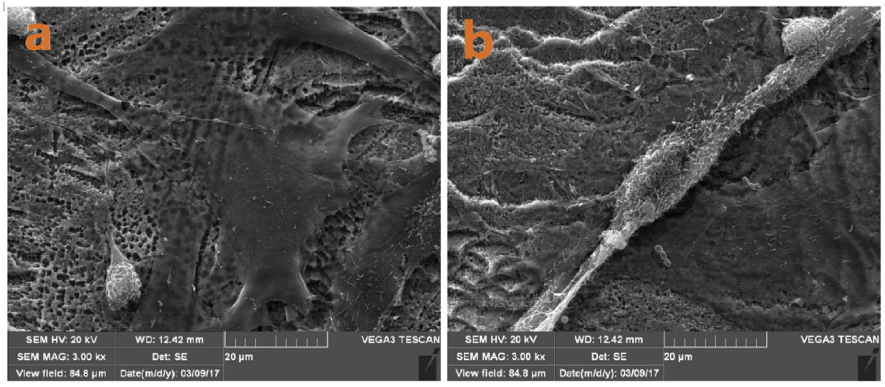

Fig. 10. a) SBF treated surfaces, b) GNP treated surfaces at the same magnification showing more cellular maturation.

in affinity and more cellular spread on titanium indicating an increase of the hydrophilicity to the titanium surface (Fig. 11).

3.5. Osteogenic gene expression

The osteogenic differentiation was assessed using quantitative real-time PCR (qPCR) after one week of cell culture to measure the gene expressions of the Col-1, OPN and late osteogenic biomarker OCN was analyzed.

Beta-actin was used as the reference gene, it was used as a positive control for the expression of Col-1, OPN and OCN (Table 7).

3.5.1. Collagen 1

The average relative gene expression of Col-1 protein was calculated from the PCR results are plotted in (Fig. 12). 1A was considered the control group. Statistical analysis is shown in (Table 8).

https://doi.org/10.1016/j.heliyon.2018.e00662
2405-8440/© 2018 Published by Elsevier Ltd. This is an open access article under the CC BY-NC-ND license (http://creativecommons.org/licenses/by-nc-nd/4.0/).

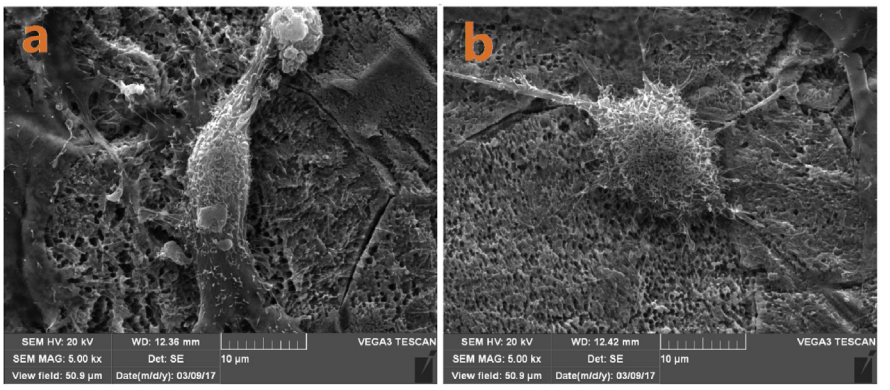

Fig. 11. a) GNP − treated surfaces, b) GNP and UV treatment showing more pronounced pseudopodia and cytoskeletal development.

Table 7. B-actin relative gene expression for different TiO_2 groups.

	1A	2A	3A	1B	2B	3B
Rat *B*-actin	19.071	18.286	18.701	18.636	19.204	18.722
	19.083	18.198	18.612	18.474	19.184	18.802
	19.066	18.341	18.588	18.681	19.339	18.843

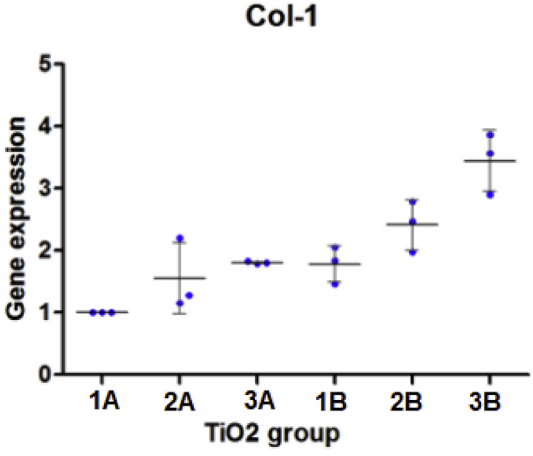

Fig. 12. Col-1 expression with the standard deviation (SD).

- **Analysis of relative gene expression of Col-1**:

The mean Col-1 expression of different groups was 1A (1.000), 2A (1.547), 3A (1.807). 1B (1.781), 2B (2.412), 3B (3.446).

Col-1 expression after one day of cell culture on the titanium plates was higher on the UV treated group (group B) than that of group A. 1B showed more Col-1 expression than 1A, 2B showed more expression than B1 and 3B also showed more expression of Col-1 than 3A. Titanium plates with SBF coating showed more expression of this

https://doi.org/10.1016/j.heliyon.2018.e00662
2405-8440/© 2018 Published by Elsevier Ltd. This is an open access article under the CC BY-NC-ND license (http://creativecommons.org/licenses/by-nc-nd/4.0/).

biomarker than the plates with no SBF treatment, while the TiO_2 plates modified with GNPs were the highest to express this gene.

3.5.1.1. Statistical analysis

Table 8. Dunnett's Multiple Comparison Test shows significant increase of Col-1 between 2B and 3B compared to the control. *indicates the level of significance. Separate t-tests shows that 3B is more significant.

Dunnett's Multiple Comparison Test	Mean diff.	q	Significance $P < 0.05$ (t- test)	Summary	95% CI of diff
1A vs 2A	−0.5467	1.811	No	ns	−1.422 to 0.3289
1A vs 3A	−0.8070	2.674	No	ns	−1.683 to 0.06860
1A vs 1B	−0.7813	2.589	No	ns	−1.657 to 0.09427
1A vs 2B	−1.412	4.679	0.0263	**	−2.288 to −0.5364
1A vs 3B	−2.446	8.104	0.0065	***	−3.321 to −1.570

**2B vs 3B:* Paired t test showed that there is a significant increase in Col-1 Expression in 3B compared to 2B with a P value of 0.0238.

3.5.2. Osteopontin

The average relative gene expression of OPN protein was calculated from the PCR results are plotted in (Fig. 13). 1A was considered the control group. Statistical analysis is shown in (Table 9).

- **Analysis of relative gene expression of osteopontin**:

The mean OPN expression of different groups was 1A (1.000), 2A (1.202), 3A (1.850). 1B (1.365), 2B (2.616), 3B (3.843).

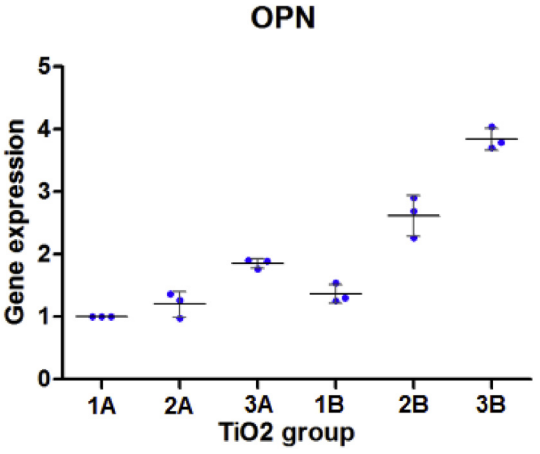

Fig. 13. OPN expression with the standard deviation (SD).

https://doi.org/10.1016/j.heliyon.2018.e00662
2405-8440/© 2018 Published by Elsevier Ltd. This is an open access article under the CC BY-NC-ND license (http://creativecommons.org/licenses/by-nc-nd/4.0/).

qPCR analysis of OPN showed that the non-PhF surfaces expressed less OPN than the UV treated groups.

3.5.2.1. Statistical analysis

Table 9. Dunnett's Multiple Comparison Test shows significant increase of OPN between 3A, 2B and 2B with the control. * indicates the level of significance. Separate t-tests shows the P values of the significant groups.

Dunnett's Multiple Comparison Test	Mean diff.	q	Significance P < 0.05 (t test)	Summary	95% CI of diff
1A vs 2A	−0.2017	1.326	No	ns	−0.6429 to 0.2395
1A vs 3A	−0.8497	5.587	yes	***	−1.291 to −0.4085
1A vs 1B	−0.3653	2.402	No	ns	−0.8065 to 0.07587
1A vs 2B	−1.616	10.63	0.0067	***	−2.057 to −1.175
1A vs 3B	−2.843	18.69	0.0006	***	−3.284 to −2.401

**2B vs 3B:* t test showed that there is a significant increase in OPN Expression in 3B compared to 2B with a P value of 0.0023.

3.5.3. Osteocalcein

The average relative gene expression of OCN protein was calculated from the PCR results are plotted in (Fig. 14). 1A was considered the control group. Statistical analysis is shown in (Table 10).

- **Analysis of relative gene expression of osteocalcin:**

The mean OCN expression of different groups was 1A (1.000), 2A (1.735), 3A (2.037). 1B (1.848), 2B (2.834), 3B (3.885).

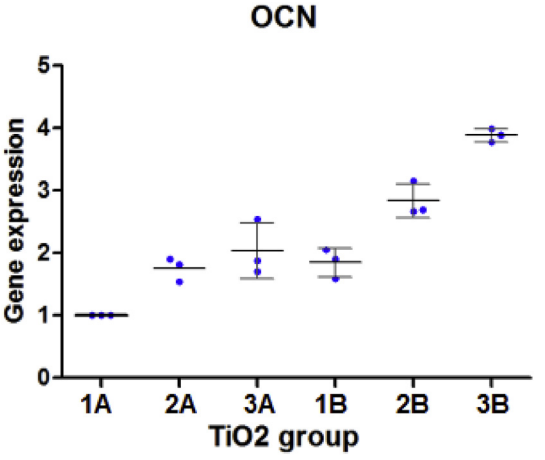

Fig. 14. OCN expression with the standard deviation (SD).

https://doi.org/10.1016/j.heliyon.2018.e00662
2405-8440/© 2018 Published by Elsevier Ltd. This is an open access article under the CC BY-NC-ND license (http://creativecommons.org/licenses/by-nc-nd/4.0/).

The expression of the OCN was similar in pattern to those expressed by Col-1 and OPN. The UV treated surfaces had a noticeably higher gene expressions than their counter groups in the none-PhF surfaces.

3.5.3.1. Statistical analysis

Table 10. Dunnett's Multiple Comparison Test shows significant increase of OCN in all groups. * indicates the level of significance. Separate t-tests shows the P values of the significant groups.

Dunnett's Multiple Comparison Test	Mean diff.	q	Significance $P < 0.05$ (t test)	Summary	95% CI of diff
A1 vs A2	−0.7523	3.941	Yes	*	−1.323 to −0.1815
A1 vs A3	−1.037	5.434	Yes	**	−1.608 to −0.4665
A1 vs B1	−0.8473	4.439	Yes	**	−1.418 to −0.2765
A1 vs B2	−1.834	9.607	0.0120	***	−2.405 to −1.263
A1 vs B3	−2.886	15.12	0.0002	***	−3.457 to −2.315

**2B vs 3B:* t test showed that there is a significant increase in OCN Expression in 3B compared to 2B with a P value of 0.0038.

3.6. ALP activity

ALP activity was measured two weeks after cell seeding onto the TiO_2 plates. The p-Nitrophenyl Phosphate (PNPP) was used a single-point photospectrometry assay via calculating the catalytic ability of ALP to hydrolyse the PNPP. It was measured by the amount of hydrolysis per square area on the TiO_2 surfaces (Fig. 15) using the IPP6.0 software.

ALP activity results following two weeks of cell seeding showed remarkable differences between the PhF TiO_2 surfaces and the non-PhF ones (Fig. 14). 3B had the highest expression among all surfaces with 20% more ALP expression than B2.

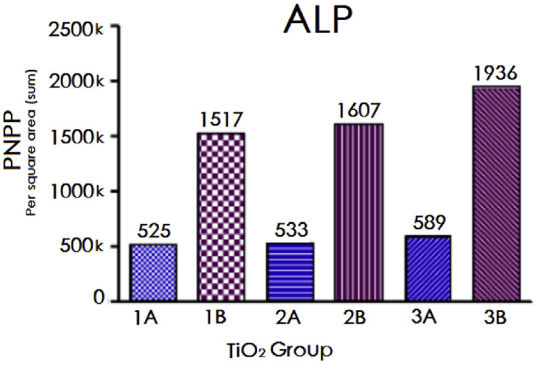

Fig. 15. ALP expression after 2 weeks of cell seeding, showing much higher results in the PhF TiO_2 groups.

https://doi.org/10.1016/j.heliyon.2018.e00662
2405-8440/© 2018 Published by Elsevier Ltd. This is an open access article under the CC BY-NC-ND license (http://creativecommons.org/licenses/by-nc-nd/4.0/).

4. Discussion

The implant's surface topography can highly affect the osseointegrative capacity and enhance the level of cellular attachment and spreading. Rougher surfaces for instance show higher osteoblastic proliferation and collagen synthesis than smooth surfaces. The biological properties can also significantly influence the cellular reactions toward the surface of the implant. For example, hydrophilic surfaces enhances osteoblastic differentiation than hydrophobic surfaces [130, 131].

Takahiro Ogawa et al. [11] used UV light to photofunctionalize the titanium surface and convert it from hydrophobic to what he called "superhydrophilic", the UV modification have also to change the surface charge from negative to positive as well as removing the surface carbons that accumulates on the TiO_2 surface resulting in a significant increase in protein absorption, osteoblastic differentiation and mineralization. It was shown that UV PhF can increase the BIC from 55% to over 98%, translating into a significant increase in primary stability and decrease in healing time. Simulated body fluid (SBF) was reported in the literature to form a hybrid micro-nano TiO_2 surface. Its ability to form a bone-like apatite layer has proved to enhance both the mechanical and biological properties [132]. Similarly, many other reports have also suggested that the increase in surface energy (hydrophilicity) does not only improve cellular function, but also leads to more expression of osteogenic biomarkers such as Col-1, OPN and ALP [133, 134, 135]. Makiko Saita et al. photofunctionalized SBF-modified titanium and found that PhF accelerated the deposition of nanoscale apatite on titanium, and the function of osteoblasts were further enhanced on the apatite-coated titanium [136]. Dohan Ehrenfest et al. found that titanium surface nanomodification has a remarkable impact on the osseointegration process by altering the molecular level via the expression of higher surface energy leading to an increase in the hydrophilicity of the surface and therefore enhancing the cellular and protein interactions on the TiO_2 surface [137]. In another study, Dong Nyoung et al. demonstrated that gold nanoparticles enhances the osteogenic differentiation of adipose derived stem cells and shows high expression of osteogenic differentiation specific markers such as COL1, Runx2, OCN, as well as high levels of alkaline phosphatase activity [138].

Collagen type I (COL-1) is the major matrix protein produced during the proliferation of osteoblasts and it is the most abundant protein in bone matrix [139, 140]. It is a good parameter of cellular differentiation but is not exclusive to osteoblastic cells, therefore, quantifying the expression of osteopontin (OPN), osteocalcin (OCN) and alkaline phosphatase (ALP) is essential. These biomarkers are more specific to bone formation and mineralization [141]. Osteopontin is a multifunctional protein linked mainly to bone metabolism and remodeling. It is produced by osteoblasts and osteoclasts and it is involved in the remodeling of bone matrix and in tissue calcification [142, 143]. Osteocalcin is produced only by osteoblasts and is involved in bone

https://doi.org/10.1016/j.heliyon.2018.e00662
2405-8440/© 2018 Published by Elsevier Ltd. This is an open access article under the CC BY-NC-ND license (http://creativecommons.org/licenses/by-nc-nd/4.0/).

metabolism [144] It is one of the main biomarkers indicating activity of osteoblasts [145]. ALP, although not specific to osteoblasts, is an essential early marker for osteoblast differentiation. It also plays a major role in the mineralization process [146].

4.1. Optical density

In our study we have created a hybrid micro-nano topography on the TiO_2 surface. The titanium plates in group 3B had all the surface treatment modalities we proposed. Results have shown a significant increase in OD for 3B group compared to the only acid etched groups, except for 2A which increased by only 6%, indicating that the hydroxyapatite layer alone has less impact on cellular differentiation and proliferation than GNPs and PhF. The OD increased by 20% in 3A compared to the control group indicating higher biocompatibility of nanoscale surfaces over not only microtopographies, but also Phf ones. The PhF-SBF plates (2B) showed higher results than those non-PhF nanotopographies indicating higher impact of UV light, 3B had a significantly more OD when compared to 2B with a p value < 0.0001, which also puts an emphasis on the GNPs effect on the cellular differentiation.

4.2. Cytotoxicity

In order to investigate the cytotoxicity of different modification modalities on the MSCs, a live/dead assay was performed. and the results showed an increased cellular viability in the following matter 1A < 2A < 3A < 1B < 2B < 3B with the number of live cells compared to total cells is roughly 50%, 55%, 60%, 65%, 70% and 80% respectively. Following 24 hours of cell seeding into TiO_2 plates, there was roughly 5% increase of the number of living cells per each modification except for a 10% increase from 2B to B3 indicating that the increased protein absorption due to PhF probably enhances the GNPs role in cellular differentiation as well. It can also be suggested that the rapid differentiation of MSCs might may contribute to the increasing ratio of live cells. Our results are in accordance to previous studies which suggested that reported cytotoxicity of GNPs can be related to their surface ligand rather than from the nanoparticles themselves [147, 148, 149]. Based on our results, we suggest that our 10 nm GNPs has less cytotoxicity than other groups and it also seemed to highly improve cellular viability.

4.3. Immunofluorescence

Confocal laser scanning microscopy was done after 24 hours of cell seeding and the immunofluorescence images showed the various osteoblast differentiation on the different titanium surfaces. PhF surfaces expressed 13% more actin fibers and 17% more vinculin than 1A which can be considered a representative of typical “as

https://doi.org/10.1016/j.heliyon.2018.e00662
2405-8440/© 2018 Published by Elsevier Ltd. This is an open access article under the CC BY-NC-ND license (http://creativecommons.org/licenses/by-nc-nd/4.0/).

received" commercial implants. There was a higher cytoskeletal development and more organized stress fibers in the SBF coated plates 2B than 2A, and in the GNP-modified 3B than 2B. This confirms the positive physiochemical effect of the UV on reversing the biological ageing of the titanium surface. Our findings comes in accordance with many previous studies regarding the ageing of TiO_2 surfaces and the reversing of this phenomena with PhF [8, 11, 12, 13, 14].

The increased cellular attachment on UV treated plates can be linked to the removal of the hydrocarbon layer on the surface of TiO_2 and to the increase in the surface energy which has been previously reported to accelerate both osteogenic differentiation of stem cells and the mineralization process [142]. The enhanced cellular spreading on all groups of TiO_2 compared to the none UV treated groups is also indicative of the newly acquired "Superhydrophilicity" of the surface.

Other treatment modalities also showed noticeable differences in cellular behavior. SBF immunofluorescent images showed higher cellular proliferation, more actin and vinculin expression and more cytoskeletal development than the none-SBF coated TiO_2 plates due to the precipitation of calcium and phosphate ions from the simulated body fluid onto the titanium to form a layer of hydroxyapatite on its surface. These findings came in accordance to the previous studies which concluded that SBF coating enhances both the biological and the mechanical properties and therefore enhances the osteoblastic differentiation [133]. The GNP modified group of titanium surfaces on the other hand showed the fastest rates of cellular differentiation, cytoskeletal maturation and associated actin and vinculin fibers expression, with 3B expressing just below 40% more actin and more than 50% vinculin compared to the control group. More mitotic activity was detected in the GNP modified surfaces. The positive biological effect of GNPs on cellular behaviour was shown to further enhance the physiochemical effect of PhF.

4.4. Surface characterization

The scanning electron microscopy (SEM) images were also taken 24 hours after the stem cells were seeded onto the titanium plates. UV treated plates showed considerable increase in the cellular activity and extracellular matrix (ECM) production compared to the none UV treated ones indicating that PhF induced an increase in the affinity of cellular and protein absorption to the TiO_2 surfaces. The hydroxyapatite coating on the SBF modified plates can be seen clearly covering the titanium micropits indicating the precipitation of the calcium and phosphate ions on the surface. This bone-like surface participates in the enhancement of the mechanical and biological properties, resulting in an enhanced cellular attachment and more cytoskeletal differentiation. 2B (UV treated) showed much more spreading due to the superhydrophilic TiO_2 surfaces. The SEM images of the GNP treated TiO_2 surfaces (3A, 3B) revealed more pronounced cellular extensions with 3B having more

https://doi.org/10.1016/j.heliyon.2018.e00662
2405-8440/© 2018 Published by Elsevier Ltd. This is an open access article under the CC BY-NC-ND license (http://creativecommons.org/licenses/by-nc-nd/4.0/).

spreading and attachment across the titanium surfaces due to the PhF effect. Previous studies have shown that the increased roughness of TiO_2 surface up-regulates the ALP activity and enhances osteoblastic differentiation but at the same time it reduces the proliferation rate compared to smooth surfaces while smooth surfaces have less effect on differentiation and more on proliferation [143, 144, 145, 146, 147, 148, 149]. This suggests that the higher cellular attachment and proliferation seen in the GNP modified TiO_2 plates in our study is not actually due to the hybrid micro-nano topography which was formed by the acid etched-hydroxyapatite coated layer but it is rather due to the GNP and the UV light effect.

The size of GNPs is reported in the literature to have various effects on cellular differentiation. D. Zhang et al. investigated the osteogenic effect of 20 nm and 40 nm GNPs differentiation and mineralization and they concluded that "size matters" and that the smaller GNPs show higher ALP activity than the larger ones [114]. Wan-Kyu and colleagues also investigated other sizes ranging from 15 to 100 nm GNPs on adipose derived stem cells and they said 30−50 nm GNPs were the most efficient [115].

We used 10 nm GNPs in our experiment, which is one of the smallest to be used for growing cells on a titanium surface and could be a key parameter for catalyzing the cellular differentiation process. The results showed that the 10 nm GNPs are very effective in promoting cellular differentiation and adhesion via increasing the protein adsorption at the nanoscale surface. Some studies have shown that nanosurfaces can interact with the osteoblasts and activate the integrin singling pathway to produce more extracellular matrix (ECM), and can also induce surface binding proteins to expose more membrane anchoring sites in the osteoblasts leading to enhanced cellular differentiation [150, 151, 152, 153, 154, 155]. Although results were more pronounced in UV treated surfaces (3B), 3A confirms the effectiveness of GNPs alone in promoting cellular differentiation is by cellular intake of the colloidal gold.

4.5. Gene expression

Previous studies have shown that GNPs can specifically and highly promote the mitogen-activated protein kinases (MAPK) pathway leading to upregulation of the Runt-related transcription factor 2 (RunX-2) which is considered the major gene in the process of osteoblastic differentiation and in turn directly promotes the expression of other osteoblastic specific genes such as Col-1, OPN and OCN [114]. This is consistent with our ECM and immunofluorescence findings which show increased ECM and pseudopodia development suggesting enhanced osteoblastic differentiation and maturation.

The results of the real time quantitative PCR have shown different levels of mRNA expression of Col-1, OPN and OCN. 1A had the least mRNA expression for the

https://doi.org/10.1016/j.heliyon.2018.e00662
2405-8440/© 2018 Published by Elsevier Ltd. This is an open access article under the CC BY-NC-ND license (http://creativecommons.org/licenses/by-nc-nd/4.0/).

three genes and was considered the control group. All the other titanium groups showed an increase in all gene expressions indicating involvement of the MAP kinase pathway and the up-regulation of the expression of the osteogenic gene Runx-2. The expression of the genes was significantly higher than the control group in the UV treated hydroxyapatite coated TiO_2 plates 2B and 3B (GNP-treated). This can be related to the increased serum protein adsorption due to the PhF effect and the GNPs combined. Previous reports highlighted that the incubation of nanomaterials results in an increased adsorption of serum proteins on the surface of the cells, and induces cellular influx of these nanoparticles through receptor-mediated endocytosis, causing them to aggregate in peri-nuclear compartments, interact with cytoplasmic proteins and activate metabolic signaling pathways [156, 157]. Despite the lack of visual detection of our GNPs due to their size we can still suggest based on these previous reports that the absorbed serum proteins on the surface of our GNPs have acted in a similar manner. This is supported by the increase in the expression of the three tested genes in group 3A indicating internalization of the 10 nm GNPs and activation of the MAPK pathway. The PCR results were further supported by the results of the ALP expression done one week after cell incubation.

4.6. Alkaline phosphatase activity

ALP is a considered an early marker of osteogenic differentiation [158] and is indicative of an ongoing mineralization process [141]. The ALP assay in our experiment was performed 2 weeks after cell incubation and it revealed remarkable differences between the PhF TiO_2 plates and the none-UV treated ones. The molecular response to UV light demonstrated by around a 3-fold increase in ALP activity in all TiO_2 groups. Therefore, we can conclude that although GNPs are very effective in triggering and enhancing the cellular differentiation cascade, the absorption and cellular internalization of GNPs largely depends on the UV enhanced protein absorption capacity of the TiO_2 surface. These PhF surfaces showed much higher cellular activity which confirms that the ageing of titanium and the resulting accumulation of surface carbon on the surface, loss of positive surface charge and hydrophilicity indeed significantly affects the speed and extent of cellular behavior as well as GNP internalization. Nevertheless, our novel hybrid micro-nanoscale hydroxyapatite-coated GNP-modified UV-treated TiO_2 surface seems to be the clear winner regarding the speed and extent of differentiation, spread, osteogenic gene expressions and even mineralization which is indicated by this high alkaline phosphatase activity.

Our attempt was to combine different treatment modalities in order to get the advantages of each and get the most biocompatible TiO_2 surface. The results show that we have largely succeeded in doing that. The new surface (3B) that we have created have shown the most cellular differentiation and proliferation within the first 24

https://doi.org/10.1016/j.heliyon.2018.e00662
2405-8440/© 2018 Published by Elsevier Ltd. This is an open access article under the CC BY-NC-ND license (http://creativecommons.org/licenses/by-nc-nd/4.0/).

hours, it showed the highest expression of osteogenic biomarkers after one week and the highest ALP expression two weeks after seeding the TiO_2 plates with the MSCs. Cellular morphology and function were significantly enhanced in 3B even when compared to the closest modality (2B). This indicates that GNPs played a vital role in this osteogenic cascade. Though we did not test for the p38-MAP Kinase signaling pathway, based on the levels of mRNA expression of the osteogenic biomarkers, we believe that the GNPs triggered the differentiation process, and it was enhanced by the increased protein absorption caused by the effect of the UV rays.

Our method showed highly enhanced cellular differentiation rates on a titanium. The new topography could further enhance the already existing "Superosseointergration" phenomenon, meaning that it can improve the bone to implant contact (BIC) ratio to more than 98% in a very short time, leading to better primary stability, less healing time, elimination of the stability dip, better anchorage for short implants and better predictability and prognosis. It could also open new treatment options in the fields of orthopedics and maxillofacial surgery for the use of screws, plates or any titanium surfaces. Further investigations should be done to evaluate the effect of this new surface on osseointegration in vivo.

5. Conclusions

We have created a novel hybrid micro-nano titanium surface with a remarkable osteogenic potential. 10 nm GNPs did not show any cytotoxicity. Immunofluorescence and SEM results showed that it highly increased the rate of differentiation, proliferation, attachment, spreading and mineralization. PCR results showed enhanced gene expressions of Col-1, OPN and OCN osteogenic markers. ALP activity was also higher than the other groups. GNPs plays an important role in cellular activity and growth. Photofunctionalizing GNPs can highly improve its ostogenic capabilities. The new topography seems to have a very high potential in enhancing osseointegration and improving outcomes for implant, maxillofacial and orthopedic patients.

Declarations

Author contribution statement

Yassir Elkhidir: Conceived and designed the experiments; Performed the experiments; Analyzed and interpreted the data; Contributed reagents, materials, analysis tools or data; Wrote the paper.

Ranfa Lai, Zhiqiang Feng: Conceived and designed the experiments; Performed the experiments; Analyzed and interpreted the data; Contributed reagents, materials, analysis tools or data.

https://doi.org/10.1016/j.heliyon.2018.e00662
2405-8440/© 2018 Published by Elsevier Ltd. This is an open access article under the CC BY-NC-ND license (http://creativecommons.org/licenses/by-nc-nd/4.0/).

Funding statement

This research did not receive any specific grant from funding agencies in the public, commercial, or not-for-profit sectors.

Competing interest statement

The authors declare no conflict of interest.

Additional information

No additional information is available for this paper.

References

[1] S.G. Steinemann, Titanium—the material of choice? Periodontol. 2000 17 (1998) 7−21.

[2] A.F. Mavrogenis, R. Dimitriou, J. Parvizi, G.C. Babis, Biology of implant osseointegration, J. Musculoskelet. Neuronal Interact. 9 (2) (2009) 61−72.

[3] M. Ramazanoglu, Y. Oshida, Osseointegration and bioscience of implant surfaces − current concepts at bone-implant interface; implant dentistry − a rapidly evolvong practice, InTech (2011).

[4] T. Ogawa, Photofunctionalization of TiO_2 for Optimal Bone-titanium Integration: a Novel Phenomenon of Superosseointegration, in: Enviromentally Benign Photocatalysts, Springer, New York, 2010, pp. 699−713.

[5] J.E. Davies, Mechanisms of endosseous integration, Int. J. Prosthodont. 11 (1998) 391−401.

[6] Y. Gao, Y. Liu, L. Zhou, et al., The effects of different wavelength UV photofunctionalization on micro-arc oxidized titanium, PLoS One 8 (7) (2013) e68086.

[7] M. Niinomi, Y. Liu, M. Nasaki, et al., Biomedical titanium alloys with Young's moduli close to that of cortical bone, Regen. Biometer. 3 (3) (2016) 173−185.

[8] J.H. Lee, T. Ogawa, The biological aging of titanium implants, Implant Dent. 21 (5) (2012) 415−421.

[9] R.B. Parkash, O. Shetty, R. Tabassum, Surface modifications of Endosseous dental implants, Int. J. Oral Implantol. Clin. Res. 3 (3) (2012) 116−121.

https://doi.org/10.1016/j.heliyon.2018.e00662
2405-8440/© 2018 Published by Elsevier Ltd. This is an open access article under the CC BY-NC-ND license (http://creativecommons.org/licenses/by-nc-nd/4.0/).

[10] T. Albrektsson, C. Johansson, Osteoinduction, osteoconduction and osseointegration, Eur. Spine J. 2 (2001) 96−101.

[11] T. Ogawa, UV photofunctionalization of titanium implants, J. Craniofac. Tissue Eng. 2 (2012) 151−158.

[12] W. Att, T. Ogawa, Biological aging of implant surfaces and their restoration with ultraviolet light treatment: a novel understanding of osseointegration, Int. J. Oral Maxillofac. Implants 27 (2012) 753−761.

[13] T. Suzuki, N. Hori, W. Att, et al., Ultraviolet treatment overcomes time-related degrading bioactivity of titanium, Tissue Eng. Part A 15 (2009) 3679−3688.

[14] F. Iwasa, N. Tsukimura, Y. Sugita, et al., TiO_2 micro-nano-hybrid surface to alleviate biological aging of UV-photofunctionalized titanium, Int. J. Nanomed. 6 (2011) 1327−1341.

[15] N. Hori, T. Ueno, T. Suzuki, et al., Ultraviolet light-treatment for the restoration of age-related degradation of titanium bioactivity, Int. J. Oral Maxillofac. Implants 25 (2010) 49−62.

[16] N. Hori, T. Ueno, H. Minamikawa, et al., Electrostatic control of protein adsorption on UV-photofunctionalized titanium, Acta Biomater. 6 (2010) 4175−4180.

[17] F. Iwasa, N. Hori, T. Ueno, et al., Enhancement of osteoblast adhesion to UV-photofunctionalized titanium via an electrostatic mechanism, Biomaterials 31 (2010) 2717−2727.

[18] B.E. Rapuano, J.J. Lee, D.E. MacDonald, Titanium alloy surface oxide modulates the conformation of adsorbed fibronectin to enhance its binding to integrins in osteoblasts, Eur. J. Oral Sci. 120 (3) (2012) 185−194.

[19] B.E. Rapuano, D.E. MacDonald, Surface oxide net charge of a titanium alloy; modulation of fibronectin-activated attachment and spreading of osteogenic cells, Colloids Surf. B Biointerfaces 82 (1) (2011) 95−103.

[20] B.E. Rapuano, K.M. Hackshaw, H.C. Schniepp, et al., Effects of coating a titanium alloy with fibronectin on the expression of osteoblast gene markers in the MC3T3 osteoprogenitor cell line, Int. J. Oral Maxillofac. Implants 27 (5) (2012) 1081−1090.

[21] J.A. Tsai, A. Lagumdzija, A. Stark, et al., Albumin-bound lipids induce free cytoplasmic calcium oscillations in human osteoblast-like cells, Cell Biochem. Funct. 25 (2007) 245−249.

https://doi.org/10.1016/j.heliyon.2018.e00662
2405-8440/© 2018 Published by Elsevier Ltd. This is an open access article under the CC BY-NC-ND license (http://creativecommons.org/licenses/by-nc-nd/4.0/).

[22] A. Klinger, D. Steinberg, D. Kohavi, et al., Mechanism of adsorption of human albumin to titanium in vitro, J. Biomed. Mater. Res. 36 (1997) 387–392.

[23] Y. Kusakawa, E. Yoshida, T. Hayakawa, Protein adsorption to titanium and zirconia using a quartz crystal microbalance method, Biomed Res. Int. (2017) 1521593.

[24] Bagambisa FB1, H.F. Kappert, W. Schilli, Cellular and molecular biological events at the implant interface, J. Craniomaxillofac. Surg. 22 (1) (1994) 12–17.

[25] D. Flanagan, Photofunctionalization of dental implants, J. Oral Implantol. 42 (5) (2016) 445–450.

[26] W. Att, N. Hori, F. Iwasa, et al., The effect of UV-photofunctionalization on the time-related bioactivity of titanium and chromium–cobalt alloys, Biomaterials 30 (26) (2009) 4268–4276.

[27] J.L. Shie, C.H. Lee, C.S. Chiou, et al., Photodegradation kinetics of formaldehyde using light sources of UVA, UVC and UVLED in the presence of composed silver titanium oxide photocatalyst, J. Hazard. Mater. 155 (2008) 164–172.

[28] H. Aita, N. Hori, M. Takeuchi, et al., The effect of ultraviolet functionalization of titanium on integration with bone, Biomaterials 30 (2009) 1015–1110.

[29] S. Suzuki, H. Kobayashi, T. Ogawa, Implant stability change and osseointegration speed of immediately loaded photofunctionalized implants, Implant Dent. 22 (5) (2013) 481–490.

[30] W. Att, N. Hori, M. Takeuchi, et al., Time-dependent degradation of titanium osteoconductivity: an implication of biological aging of implant materials, Biomaterials 30 (2009) 5352–5363.

[31] F. Iwasa, K. Baba, T. Ogawa, Enhanced intracellular signaling pathway in osteoblasts on ultraviolet lighttreated hydrophilic titanium, Biomed. Res. 37 (1) (2016) 1–11.

[32] L. Le Guehennec, A. Soueidan, P. Layrolle, et al., Surface treatments of titanium dental implants for rapid osseointegration, Dent. Mater. 23 (2007) 844–854.

[33] N. Sykaras, A.M. Iacopino, V.A. Marker, et al., Implant materials, designs, and surface topographies: their effect on osseointegration. A literature review, Int. J. Oral Maxillofac. Implants 15 (2000) 675–690.

[34] J.T. Parsons, A.R. Horwitz, M.A. Schwartz, Cell adhesion: integrating cytoskeletal, dynamics and cellular tension, Nat. Rev. Mol. Cell Biol. 11 (9) (2010) 633–643.

 https://doi.org/10.1016/j.heliyon.2018.e00662
2405-8440/© 2018 Published by Elsevier Ltd. This is an open access article under the CC BY-NC-ND license (http://creativecommons.org/licenses/by-nc-nd/4.0/).

[35] J.D. Humphries, P. Wang, C. Streuli, B. Geiger, M.J. Humphries, C. Ballestrem, Vinculin controls focal adhesion formation by direct interactions with talin and actin, J. Cell Biol. 179 (2007) 1043−1057.

[36] K.K. Wen, P.A. Rubenstein, K.A. Demali, Vinculin nucleates actin polymerization and modifies actin filament structure, J. Biol. Chem. 284 (44) (2009) 30463−30473.

[37] J.E. Ellingsen, A study on the mechanism of protein adsorption to TiO_2, Biomaterials 12 (1991) 593−596.

[38] W.H. Goldmann, D.E. Ingber, Intact vinculin protein is required for control of cell shape, cell mechanics, and rac-dependent lamellipodia formation, Biochem. Biophys. Res. Commun. 290 (2002) 749−755.

[39] R.M. Ezzell, W.H. Goldmann, N. Wang, et al., Vinculin promotes cell spreading by mechanically coupling integrins to the cytoskeleton, Exp. Cell Res. 231 (1997) 14−26.

[40] A. Mata, X. Su, A.J. Fleischman, et al., Osteoblast attachment to a textured surface in the absence of exogenous adhesion proteins, IEEE Trans. Nanobiosci. 2 (2003) 287−294.

[41] H.A. Pols, H.P. Schilte, P.J. Nijweide, T.J. Visser, J.C. Birkenhager, The influence of albumin on vitamin D metabolism in fetal chick osteoblast-like cells, Biochem. Biophys. Res. Commun. 125 (1984) 265−272.

[42] M. Al-Jawad, G. Fragneto, J. Liu, et al., Fibronectin adsorption studied using neutron reflectometry and complementary techniques, Eur. Phys. J. E. Soft Matter 30 (2009) 175−179.

[43] J.L. Dewez, A. Doren, Y.J. Schneider, et al., Competitive adsorption of proteins: key of the relationship between substratum surface properties and adhesion of epithelial cells, Biomaterials 20 (1999) 547−559.

[44] C.J. Pendegrass, M. El-Husseiny, G.W. Blunn, The development.of fibronectin-functionalised hydroxyapatite coatings to improve dermal fibroblast attachment in vitro, J. Bone Jt. Surg. Br. 94 (2012) 564−569.

[45] Z. Mischa, A. Darren, R.A. Morgan, et al., The role of albumin and fibronectin in the adhesion of fibroblasts to plasma polymer surfaces, Plasma Process. Polym. 9 (2011) 149−156.

[46] Y. Arima, H. Iwata, Effect of wettability and surface functional groups on protein adsorption and cell adhesion using well-defined mixed self-assembled monolayers, Biomaterials 28 (2007) 3074−3082.

https://doi.org/10.1016/j.heliyon.2018.e00662
2405-8440/© 2018 Published by Elsevier Ltd. This is an open access article under the CC BY-NC-ND license (http://creativecommons.org/licenses/by-nc-nd/4.0/).

[47] K. Miyata, J. Takebe, Anodized-hydrothermally treated titanium with a nano-topographic surface structure regulates integrin-α6β4 and laminin-5 gene expression in adherent murine gingival epithelial cells, J. Prosthodont. Res. 57 (2013) 99−108.

[48] E.M. Bik, C.D. Long, G.C. Amitage, et al., Bacterial diversity in the oral cavity of 10 healthy individuals, ISME J. 4 (8) (2010) 962−1047.

[49] J.F. Siqueira Jr., A.F. Fouad, I.N. Rocas, Pyrosequencing as a tool for better understanding of human microbiomes, J. Oral Microbiol. (2012) 4.

[50] S.H. Safii, R.M. Palmer, R.F. Wilson, Risk of implant failure and marginal bone loss in subjects with a history of periodontitis: a systematic review and metaanalysis, Clin. Implant Dent. Relat. Res. 12 (2010) 165−174.

[51] A. Mombelli, N. Muller, N. Cionca, The epidemiology of peri-implantitis, Clin. Oral Implants Res. 23 (6) (2012) 67−76.

[52] L. Jin, W. Guo, P. Xue, et al., Quantitative assay for the colonization ability of heterogeneous bacteria on controlled nanopillar structures, Nanotechnology 26 (2015) 055702.

[53] I.M. Cavalcanti, A.P. Ricomini Filho, S.C. Lucena-Ferreira, W.J. Da Silva, A.F. Paes Leme, P.M. Senna, et al., Salivary pellicle composition and multi-species biofilm developed on titanium nitrided by cold plasma, Arch. Oral Biol. 59 (2014) 695−703.

[54] L. Badihi Hauslich, M.N. Sela, D. Steinberg, et al., The adhesion of oral bacteria to modified titanium surfaces: role of plasma proteins and electrostatic forces, Clin. Oral Implants Res. 24 (A100) (2013) 49−56.

[55] D.J. Rileya, V. Bavastrelloa, U. Covanib, A. Baroneb, N. Nicolinia, An in-vitro study of the sterilization of titanium dental implants using low intensity, Dent. Mater. 21 (8) (2005) 756−760.

[56] E. Einarsson, S.G. Svard, et al., UV irradiation responses in Giardia intestinalis, Exp. Parasitol. 154 (2015) 25−32.

[57] F. Barbut, How to eradicate Clostridium difficile from the environment, J. Hosp. Infect. 89 (4) (2015) 287−295.

[58] C.S. Enwemeka, D. Williams, S.K. Enwemeka, et al., Blue 470-nm light kills methicillin-resistant Staphylococcus aureus (MRSA) in vitro, Promot. Laser Surg. 27 (2) (2009) 221−226.

[59] A.M. Gallardo-Moreno, M.A. Pacha-Olivenza, L. Saldana, et al., In vitro biocompatibility and bacterial adhesion of physico-chemically modified

https://doi.org/10.1016/j.heliyon.2018.e00662
2405-8440/© 2018 Published by Elsevier Ltd. This is an open access article under the CC BY-NC-ND license (http://creativecommons.org/licenses/by-nc-nd/4.0/).

Ti6Al4V surface by means of UV irradiation, Acta Biomater. 5 (1) (2009) 181−192.

[60] Y. Yamada, M. Yamada, T. Ueda, et al., Reduction of biofilm formation on titanium surface with ultraviolet-C pre-irradiation, Biomater. Appl. 29 (2) (2014) 161−171.

[61] E.D. De Avila, B.F. Lima, T. Sekiya, et al., Effect of UV-photofunctionalization on oral bacterial attachment and biofilm formation to titanium implant material, Biomaterials 67 (2015) 84−92.

[62] M. Hirota, T. Ozawa, T. Iwai, et al., Implant stability development of photo-functionalized implants placed in regular and complex cases: a case-control study, Int. J. Oral Maxillofac. Implants 31 (3) (2016) 676−686.

[63] A. Funato, M. Yamada, T. Ogawa, Success rate, healing time, and implant stability of photofunctionalized dental implants, Int. J. Oral Maxillofac. Implants 28 (5) (2013) 1261−1271.

[64] T. Ogawa, Photofunctionalization of TiO_2 for Optimal Integration of Titanium with Bone, in: Applications of Titanium Oxide-based Materials. Benign Photocatalysts, Springer, 2010, pp. 699−713.

[65] N. Meredith, D. Alleyne, P. Cawley, Quantitative determination of the stability of the implant-tissue interface using resonance frequency analysis, Clin. Oral Implants Res. 7 (1996) 261−267.

[66] H.L. Huang, M.T. Tsai, K.C. Su, et al., Relation between initial implant stability quotient and bone-implant contact percentage: an in vitro model study, Oral Surg. Oral Med. Oral Pathol. Oral Radiol. 116 (5) (2013) 356−361.

[67] K.J. Park, J.Y. Kwon, S.K. Kim, et al., The relationship between implant stability quotient values and implant insertion variables: a clinical study, J. Oral Rehabil. 39 (2012) 151−159.

[68] T. Ueno, M. Yamada, T. Suzuki, et al., Enhancement of bone-titanium integration profile with UV-photofunctionalized titanium in a gap healing model, Biomaterials 31 (2010) 1546−1557.

[69] I. Nishimura, Y. Huang, F. Butz, et al., Discrete deposition of hydroxyapatite nanoparticles on a titanium implant with predisposing substrate microtopography accelerated osseointegration, Nanotechnology 18 (2007) 1−9.

[70] G. Mendonca, D.B. Mendonca, F.J. Aragao, et al., Advancing dental implant surface technology—from micron- to nanotopography, Biomaterials 29 (2008) 3822−3835.

https://doi.org/10.1016/j.heliyon.2018.e00662
2405-8440/© 2018 Published by Elsevier Ltd. This is an open access article under the CC BY-NC-ND license (http://creativecommons.org/licenses/by-nc-nd/4.0/).

[71] Ikeda T1, Y. Hagiwara, M. Hirota, et al., Effect of photofunctionalization on fluoride-treated nanofeatured titanium, J. Biomater. Appl. 28 (8) (2014) 1200−1212.

[72] N. Tsukimura, T. Ueno, F. Iwasa, et al., Bone integration capability of alkali- and heat-treated nanobimorphic Ti-15Mo-5Zr-3Al, Acta Biomater. 7 (2011) 4267−4277.

[73] L.M. Svanborg, M. Andersson, A. Wennerberg, Surface characterization of commercial oral implants on the nanometer level, J. Biomed. Mater. Res. B Appl. Biomater. 92 (2010) 462−469.

[74] K. Kubo, N. Tsukimura, F. Iwasa, et al., Cellular behavior on TiO_2 nanonodular structures in a micro-to-nanoscale hierarchy model, Biomaterials 30 (2009) 5319−5329.

[75] D.N. Heo, W.K. Ko, H.R. Lee, et al., Titanium dental implants surface-immobilized with gold nanoparticles as osteoinductive agents for rapid osseointegration, J. Colloid Interface Sci. 469 (2016) 129−137.

[76] C. Sanchez, H. Arribart, M.M. Guille, Biomimetism and bioinspiration as tools for the design of innovative materials and systems, Nat. Mater. 4 (2005) 277−288.

[77] J.P. Spatz, Nano- and micropatterning by organic−inorganic templating of hierarchical self-assembled structures, Angew Chem. Int. Ed. Engl. 41 (2002) 3359−3362.

[78] M.J. Dalby, N. Gadegaard, A.S. Curtis, et al., Nanotopographical control of human osteoprogenitor differentiation, Curr. Stem Cell Res. Ther. 2 (2007) 129−138.

[79] M. Jager, C. Zilkens, K. Zanger, et al., Significance of nano- and microtopography for cell-surface interactions in orthopaedic implants, J. Biomed. Biotechnol. 8 (2007) 69036.

[80] T. Ueno, N. Tsukimura, M. Yamada, et al., Enhanced boneintegration capability of alkali- and heat-treated nanopolymorphic titanium in micro-to-nanoscale hierarchy, Biomaterials 32 (2011) 7297−7308.

[81] T. Ogawa, L. Saruwatari, K. Takeuchi, et al., Ti nano-nodular structuring for bone integration and regeneration, J. Dent. Res. 87 (2008) 751−756.

[82] L.H. Li, Y.M. Kong, H.W. Kim, et al., Improved biological performance of Ti implants due to surface modification by micro-arc oxidation, Biomaterials 25 (2004) 2867−2875.

https://doi.org/10.1016/j.heliyon.2018.e00662
2405-8440/© 2018 Published by Elsevier Ltd. This is an open access article under the CC BY-NC-ND license (http://creativecommons.org/licenses/by-nc-nd/4.0/).

[83] Y.W. Lim, S.Y. Kwon, D.H. Sun, H.E. Kim, Y.S. Kim, Enhanced cell integration to titanium alloy by surface treatment with microarc oxidation: a pilot study, Clin. Orthop. Relat. Res. 467 (2009) 2251−2258.

[84] O. Jeon, E. Alsberg, Photofunctionalization of Alginate hydrogels to promote adhesion and proliferation of human mesenchymal stem cells, Tissue Eng. A19 (2013) 11−12.

[85] H. Aita, W. Att, T. Ueno, et al., Ultraviolet light-mediated photofunctionalization of titanium to promote human mesenchymal stem cell migration, attachment, proliferation and differentiation, Acta Biomater. 5 (8) (2009) 3247−3257.

[86] M. Tabuchi, T. Ikeda, M. Hirota, et al., Effect of UV photofunctionalization on biologic and anchoring capability of orthodontic miniscrews, Int. J. Oral Maxillofac. Implants 30 (4) (2015) 868−879.

[87] A.G. Crismani, M.H. Bertl, A.G. Celar, et al., Miniscrews in orthodontic treatment: review and analysis of published clinical trials, Am. J. Orthod. Dentofac. Orthop. 137 (1) (2010) 108−113.

[88] M. Hirota, T. Ikeda, M. Tabuchi, et al., Effect of ultraviolet-mediated photofunctionalization for bone formation around medical titanium mesh, J. Oral Maxillofac. Surg. 72 (9) (2014) 1691−1702.

[89] K. Matsuura, R. Utoh, K. Nagase, et al., Cell sheet approach for tissue engineering and regenerative medicine, J Contr. Release 190 C (2014) 228−239.

[90] M. Ishijima, M. Hirota, W. Park, et al., Osteogenic cell sheets reinforced with photofunctionalized micro-thin titanium, J. Biomater. Appl. 29 (10) (2015) 1372−1384.

[91] Z. Zhang, K. Wang, C. Bai, et al., The influence of UV irradiation on the biological properties of MAO-formed ZrO_2, Colloids Surf. B Biointerfaces 89 (2012) 40−47.

[92] V. Sollazzo, F. Pezzetti, A. Scarano, et al., Zirconium oxide coating improves implant osseointegration in vivo, Dent. Mater. 24 (3) (2008) 357−361.

[93] T. Tuna, M. Wein, M. Swain, et al., Influence of ultraviolet photofunctionalization on the surface characteristics of zirconia-based dental implant materials, Dent. Mater. 31 (2) (2015) 14−24.

[94] J. Chevalier, What future for zirconia as a biomaterial? Biomaterials 27 (2006) 535−543.

https://doi.org/10.1016/j.heliyon.2018.e00662
2405-8440/© 2018 Published by Elsevier Ltd. This is an open access article under the CC BY-NC-ND license (http://creativecommons.org/licenses/by-nc-nd/4.0/).

[95] J. Chevalier, J. Loh, L. Gremillard, et al., Low-temperature degradation in zirconia with a poroussurface, Acta Biomater. 7 (2011) 2986−2993.

[96] W. Att, M. Takeuchi, T. Suzuki, et al., Enhanced osteoblast function on ultraviolet light-treated zirconia, Biomaterials 30 (7) (2009) 1273−1280.

[97] Y. Han, Y. Yan, C. Lu, Ultraviolet-enhanced bioactivity of ZrO_2 films prepared by micro-arc oxidation, Thin Solid Films 517 (5) (2009) 1577−1581.

[98] D.A. Giljohann, D.S. Seferos, W.L. Daniel, et al., Gold nanoparticles for biology and medicine, Angew Chem. Int. Ed. Engl. 49 (19) (2010 Apr 26) 3280−3294.

[99] L. Dykman, N. Khlebtsov, Gold nanoparticles in biomedical applications: recent advances and perspectives, Chem. Soc. Rev. 41 (6) (2012 Mar 21) 2256−2282.

[100] Boisselier E1, D. Astruc, Gold nanoparticles in nanomedicine: preparations, imaging, diagnostics, therapies and toxicity, Chem. Soc. Rev. 38 (6) (2009 Jun) 1759−1782.

[101] P. Ghosh, G. Han, M. De, et al., Gold nanoparticles in delivery applications, Adv. Drug Deliv. Rev. 60 (2008) 1307−1315.

[102] L.A. Dykman, N.G. Khlebtsov, Immunological properties of gold nanoparticles, Sci. Chem. Sci. 8 (3) (2017 Mar 1) 1719−1735.

[103] A. Kumar, X. Zhang, X.-J. Liang, Gold nanoparticles: emerging paradigm for targeted drug delivery system, Biotechnol. Adv. 31 (2013) 593−606.

[104] K. Niikura, T. Matsunaga, T. Suzuki, et al., Gold nanoparticles as a vaccine platform: influence of size and shape on immunological responses in vitro and in vivo, ACS Nano 7 (2013) 3926−3938.

[105] C. Yi, D. Liu, C.-C. Fong, et al., Gold nanoparticles promote osteogenic differentiation of mesenchymal stem cells through p38 MAPK pathway, ACS Nano 4 (2010) 6439−6448.

[106] Q.X. Mu, D.L. Broughton, et al., Endosomal leakage and nuclear translocation of multiwalled carbon nanotubes: developing a model for cell uptake, Nano Lett. 9 (2009) 4370−4375.

[107] A.E. Porter, M. Gass, J.S. Bendall, et al., Uptake of noncytotoxic acid-treated single-walled carbon nanotubes into the cytoplasm of human macrophage cells, ACS Nano 3 (2009) 1485−1492.

https://doi.org/10.1016/j.heliyon.2018.e00662
2405-8440/© 2018 Published by Elsevier Ltd. This is an open access article under the CC BY-NC-ND license (http://creativecommons.org/licenses/by-nc-nd/4.0/).

[108] G. Xiao, D. Jiang, P. Thomas, et al., MAPK pathways activate and phosphorylate the osteoblast-specific transcription factor, Cbfa1, J. Biol. Chem. 275 (2000) 4453−4459.

[109] R.K. Jaiswal, N. Jaiswal, S.P. Bruder, et al., Adult human mesenchymal stem cell differentiation to the osteogenic or adipogenic lineage is regulated by mitogen-activated protein kinase, J. Biol. Chem. 275 (2000) 9645−9652.

[110] P.G. Ziros, A.P. Gil, T. Georgakopoulos, et al., The bone- specific transcriptional regulator Cbfa1 is a target of mechanical signals in osteoblastic cells, J. Biol. Chem. 277 (2002) 23934−23941.

[111] D. Liu, J. Zhang, C. Yi, et al., The effects of gold nanoparticles on the proliferation, differentiation, and mineralization function of MC3T3-E1 cells in vitro, Chin. Sci. Bull. 55 (2010) 1013−1019.

[112] O.-J. Sul, J.-C. Kim, T.-W. Kyung, et al., Gold nanoparticles inhibited the receptor activator of nuclear factor-κb ligand (RANKL)-induced osteoclast formation by acting as an antioxidant, Biosci. Biotechnol. Biochem. 74 (2010) 2209.

[113] C.Q. Yi, C.C. Fong, W.W. Chen, et al., Interactions between carbon nanotubes and DNA polymerase and restriction endonucleases, Nanotechnology 18 (2007) 025102.

[114] D. Zhang, D. Liu, J. Zhang, et al., Gold nanoparticles stimulate differentiation and mineralization of primary osteoblasts through the ERK/MAPK signaling pathway, Mater. Sci. Eng. C 42 (2014) 70−77.

[115] W.K. Ko, D.N. Heo, et al., The effect of gold nanoparticle size on osteogenic differentiation of adipose-derived stem cells, J. Colloid Interface Sci. 438 (2015) 68−76.

[116] T. Miyaza, H.M. Kim, T. Kokubo, et al., Mechanism of bonelike apatite formation on bioactive tantalum metal in a simulated body fluid, Biomaterials 23 (3) (2002) 827−832.

[117] X.X. Wang, S. Hayakawa, K. Tsuru, et al., A comparative study of in vitro apatite deposition on heat-, H(2)O(2)-, and NaOH-treated titanium surfaces, J. Biomed. Mater. Res. 54 (2) (2001) 172−178.

[118] T. Kokubo, H. Takadama, How useful is SBF in predicting in vivo bone bioactivity? Biomaterials 27 (2006) 2907−2915.

[119] H.M. Kim, F. Miyaji, T. Kokubo, et al., Bonding strength of bone-like apatite layer to Ti metal substrate, J. Biomed. Mater. Res. 38 (2) (1997) 121−127.

https://doi.org/10.1016/j.heliyon.2018.e00662
2405-8440/© 2018 Published by Elsevier Ltd. This is an open access article under the CC BY-NC-ND license (http://creativecommons.org/licenses/by-nc-nd/4.0/).

[120] E. Ajami, K.F. Aguey-Zinsou, Calcium phosphate growth at electropol-ished titanium surfaces, J. Funct. Biomater. 3 (2) (2012) 327−348.

[121] H. Havitcioglu, B. Cecen, A. Pasinli, et al., In vivo investigation of calcium phosphate coatings on Ti6-Al-4V alloy sub-strates using lactic acid − sodium lactate buffered synthetic body fluid, Acta Orthop. Traumatol. Turc. 47 (6) (2013) 417−422.

[122] E. Sandrini, C. Giordano, V. Busini, et al., Apatite formation and cellular response of a novel bioactive titanium, J. Mater. Sci. Mater. Med. 18 (6) (2007) 1225−1237.

[123] T. Kokubo, H.M. Kim, M. Kawashita, et al., Bioactive metals: preparation and properties, J. Mater. Sci. Mater. Med. 15 (2) (2004) 99−107.

[124] L. Moroni, P.M. Fornasari, Human mesenchymal stem cells: a bank perspective on the isolation, characterization and potential of alternative sources for the regeneration of musculoskeletal tissues, J. Cell. Physiol. 228 (2013) 680−687.

[125] L. Wu, X. Cai, S. Zhang, et al., Regeneration of articular cartilage by adipose tissue derived mesenchymal stem cells: perspective from stem cell biology and molecular medicine, J. Cell. Physiol. 228 (2013) 938−944.

[126] Anita H. Undale, Jennifer J. Westendorf, Mesenchymal stem cells for bone repair and metabolic bone diseases, Mayo Clin. Proc. 84 (10) (2009 Oct) 893−902.

[127] Yunhao Qin, Junjie Guan, Changqing Zhang, Mesenchymal stem cells: mechanisms and role in bone regeneration, Postgrad. Med. J. 90 (1069) (2014 Nov) 643−647.

[128] Y. Yue, X. Yang, X. Wei, et al., Osteogenic differentiation of adipose-derived stem cells prompted by low-intensity pulsed ultrasound, Cell Prolif. 46 (2013) 320−327.

[129] L. Liu, W. Yuan, J. Wang, Mechanisms for osteogenic differentiation of human mesenchymal stem cells induced by fluid shear stress, Biomech. Model Mechanobiol. 9 (2010) 659−670.

[130] N. Wei, S. Bin, Z. Jing, et al., Influence of implant surface topography on bone-regenerative potential and mechanical retention in the human maxilla and mandible, Am. J. Dent. 27 (3) (2014 Jun) 171−176.

[131] A. Wennerberg, T. Albrektsson, Effects of titanium surface topography on bone integration: a systematic review, Clin. Oral Implants Res. 20 (Suppl. 4) (2009 Sep) 172−184.

https://doi.org/10.1016/j.heliyon.2018.e00662
2405-8440/© 2018 Published by Elsevier Ltd. This is an open access article under the CC BY-NC-ND license (http://creativecommons.org/licenses/by-nc-nd/4.0/).

[132] J. Hao, Y. Li, B. Li, et al., Biological and mechanical effects of micro-nanostructured titanium surface on an osteoblastic cell line in vitro and osteointegration in vivo, Appl. Biochem. Biotechnol. (2017 Mar 20).

[133] J.Y. Lim, M.C. Shaughnessy, Z. Zhou, et al., Surface energy effects on osteoblast spatial growth and mineralization, Biomaterials 29 (2008) 1776−1784.

[134] H.C. Lai, L.F. Zhuang, X. Liu, et al., The influence of surface energy on early adherent events of osteoblast on titanium substrates, J. Biomed. Mater. Res. A 93 (2010) 289−296.

[135] Z. Qu, X. Rausch-Fan, M. Wieland, et al., The initial attachment and subsequent behavior regulation of osteoblasts by dental implant surface modification, J. Biomed. Mater. Res. A 82 (2007) 658−668.

[136] Makiko Saita, Takayuki Ikeda, et al., UV photofunctionalization promotes nano-biomimetic apatite deposition on titanium, Int. J. Nanomed. 11 (2016) 223−234.

[137] D.M. Dohan Ehrenfest, P.G. Coelho, B.S. Kang, et al., Classification of osseointegrated implant surfaces: materials, chemistry and topography, Trends Biotechnol. 28 (4) (2010) 198−206.

[138] J. Li, J.J. Li, J. Zhang, et al., Gold nanoparticle size and shape influence on osteogenesis of mesenchymal stem cells, Nanoscale 8 (15) (2016 Apr 21) 7992−8007.

[139] Karl E. Kadler, David F. Holmes, John A. Trotter, et al., Collagen fibril formation, Biochem. J. 316 (1) (May 15, 1996) 1−11.

[140] Morteza Mahmoudi, Iseult Lynch, Mohammad Reza Ejtehadi, et al., Protein−nanoparticle interactions: opportunities and challenges, Chem. Rev. 111 (9) (2011) 5610−5637.

[141] Luis A. Castillo Diaz, Mohamed Elsawy, et al., Osteogenic differentiation of human mesenchymal stem cells promotes mineralization within a biodegradable peptide hydrogel, J. Tissue Eng. (2016 Jan-Dec) 7.

[142] Carolina De Fusco, Antonietta Messina, et al., Osteopontin: relation between adipose tissue and bone homeostasis, Stem Cells Int (2017) 4045238.

[143] A.N. Kothari, M.L. Arffa, V. Chang, et al., Osteopontin—a master regulator of epithelial-mesenchymal transition, J. Clin. Med. 5 (4) (2016) 39.

[144] N.K. Lee, H. Sowa, E. Hinoi, et al., Endocrine regulation of energy metabolism by the skeleton, Cell 130 (3) (Aug 2007) 456−469.

 https://doi.org/10.1016/j.heliyon.2018.e00662
2405-8440/© 2018 Published by Elsevier Ltd. This is an open access article under the CC BY-NC-ND license (http://creativecommons.org/licenses/by-nc-nd/4.0/).

[145] S. Bharadwaj, A.G. Naidu, G.V. Betageri, et al., Milk ribonuclease-enriched lactoferrin induces positive effects on bone turnover markers in postmenopausal women, Osteoporos. Int. 20 (9) (Sep 2009) 1603−1611.

[146] K. Štefková, J. Procházková, J. Pacherník, Alkaline phosphatase in stem cells, Stem Cell. Int. 2015 (2015) 628368.

[147] C. Grabinski, N. Schaeublin, A. Wijaya, et al., Effect of gold nanorod surface chemistry on cellular response, ACS Nano 5 (2011) 2870−2879.

[148] D.N. Heo, W.K. Ko, H.J. Moon, et al., Inhibition of osteoclast differentiation by gold nanoparticles functionalized with cyclodextrin curcumin complexes, ACS Nano 8 (2014) 12049−12062.

[149] S. Suarasan, M. Focsan, O. Soritau, et al., One-pot, green synthesis of gold nanoparticles by gelatin and investigation of their biological effects on osteoblast cells, Colloids Surf. B 132 (2015) 122−131.

[150] I. Wall, N. Donos, K. Carlqvist, et al., Modified titanium surfaces promote accelerated osteogenic differentiation of mesenchymal stromal cells in vitro, Bone 45 (2009) 17−26.

[151] K. Kieswetter, Z. Schwartz, T.W. Hummert, et al., Surface roughness modulates the local production of growth factors and cytokines by osteoblast-like MG-63 cells, J. Biomed. Mater. Res. 32 (1996) 55−63.

[152] R. Olivares-Navarrete, S.L. Hyzy, D.L. Hutton, et al., Direct and indirect effects of microstructured titanium substrates on the induction of mesenchymal stem cell differentiation towards the osteoblast lineage, Biomaterials 31 (2010) 2728−2735.

[153] Z. Schwartz, C.H. Lohmann, J. Oefinger, et al., Implant surface characteristics modulate differentiation behavior of cells in the osteoblastic lineage, Adv. Dent. Res. 13 (1999) 38−48.

[154] S. Lossdorfer, Z. Schwartz, L. Wang, et al., Microrough implant surface topographies increase osteogenesis by reducing osteoclast formation and activity, J. Biomed. Mater. Res. A 70 (2004) 361−369.

[155] J. Lincks, B.D. Boyan, C.R. Blanchard, et al., Response of MG63 osteoblast-like cells to titanium and titanium alloy is dependent on surface roughness and composition, Biomaterials 19 (1998) 2219−2232.

[156] R. Batzer, Y. Liu, D.L. Cochran, et al., Prostaglandins mediate the effects of titanium surface roughness on MG63 osteoblast-like cells and alter cell responsiveness to 1α,25-(OH)2D3, J. Biomed. Mater. Res. 41 (1998) 489−496.

 https://doi.org/10.1016/j.heliyon.2018.e00662
2405-8440/© 2018 Published by Elsevier Ltd. This is an open access article under the CC BY-NC-ND license (http://creativecommons.org/licenses/by-nc-nd/4.0/).

[157] B.D. Boyan, R. Batzer, K. Kieswetter, et al., Titanium surface roughness alters responsiveness of MG63 osteoblast-like cells to 1α,25-(OH)2D3, J. Biomed. Mater. Res. 39 (1998) 77−85.

[158] E. Palin, H. Liu, T. Webster, Mimicking the nanofeatures of bone increases bone-forming cell adhesion and proliferation, Nanotechnology 16 (2005) 9.

https://doi.org/10.1016/j.heliyon.2018.e00662
2405-8440/© 2018 Published by Elsevier Ltd. This is an open access article under the CC BY-NC-ND license (http://creativecommons.org/licenses/by-nc-nd/4.0/).